Interactions of the "Piano-stool" [Ruthenium(II) (η^6-arene)(en)Cl]$^+$ Complexes With Water and Nucleobases; ab initio and DFT Study

ZDENĚK FUTERA,[1] JULIA KLENKO,[1] JUDIT E. ŠPONER,[2] JIŘÍ ŠPONER,[2] JAROSLAV V. BURDA[1]
[1]*Department of Chemical Physics and Optics, Faculty of Mathematics and Physics, Charles University, Ke Karlovu 3, 121 16 Prague 2, Czech Republic*
[2]*Institute of Biophysics, Academy of Sciences of the Czech Republic, v.v.i., Kralovopolská 135, 612 65 Brno, Czech Republic*

Received 14 May 2008; Revised 23 October 2008; Accepted 24 October 2008
DOI 10.1002/jcc.21179
Published online 17 December 2008 in Wiley InterScience (www.interscience.wiley.com).

Abstract: Piano stool ruthenium complexes of the composition [Ru(II)(η^6-arene)(en)Cl]$^{+/2+}$ (en = ethylenediamine) represent an emerging class of cisplatin-analogue anticancer drug candidates. In this study, we use computational quantum chemistry to characterize the structure, stability and reactivity of these compounds. All these structures were optimized at DFT(B3LYP)/6-31G(d) level and their single point properties were determined by the MP2/6-31++G(2df,2pd) method. Thermodynamic parameters and rate constants were determined for the aquation process, as a replacement of the initial chloro ligand by water and subsequent exchange reaction of aqua ligand by nucleobases. The computations were carried out at several levels of DFT and ab initio theories (B3LYP, MP2 and CCSD) utilizing a range of bases sets (from 6-31G(d) to aug-cc-pVQZ). Excellent agreement with experimental results for aquation process was obtained at the CCSD level and reasonable match was achieved also with the B3LYP/6-31++G(2df,2pd) method. This level was used also for nucleobase-water exchange reaction where a smaller rate constant for guanine exchange was found in comparison with adenine. Although adenine follows a simple replacement mechanism, guanine complex passes by a two-step mechanism. At first, Ru-O6(G) adduct is formed, which is transformed through a chelate TS2 to the Ru-N7(G) final complex. In case of guanine, the exchange reaction is more favorable thermodynamically (releasing in total by about 8 kcal/mol) but according to our results, the rate constant for guanine substitution is slightly smaller than the analogous constant in adenine case when reaction course from local minimum is considered.

 J Comput Chem 30: 1758–1770, 2009

Key words: piano-stool Ruthenium complexes; DFT calculations; thermodynamic parameters; rate constants

Introduction

Because cisplatin was discovered as a potent anticancer agent, an intense search for other metallocomplexes is being pursued. The reason stems from the fact that cisplatin is very toxic, has many side effects, and is not active for all kinds of carcinomas. Nowadays many transition metals are known as possible antitumor drugs. Many experimental studies appeared on complexes of titanium,[1–4] rhodium,[5–9] ruthenium,[10–20] and other metals,[21,22] which are active against cancer cells, exploring various biophysical and biochemical properties. Soon after these reports, theoretical calculations also followed supporting experimental facts with molecular description of possible reactions of these complexes.

A lot of effort was devoted to e.g., theoretical description of the effects of cisplatin and its derivatives.[23–29] Some studies concerned the aquation process of metallocomplexes, which is crucial in the process of their activation,[30–37] interactions with purine DNA bases[38–49] or other competitive cellular components, such as side chains of amino acids.[50,51]

Ruthenium compounds represent another important family of the explored complexes which attracted substantial interest in the recent computational chemistry literature.[18,43,52–54] Many

Additional Supporting Information may be found in the online version of this article.

Correspondence to: J. V. Burda; e-mail: burda@karlov.mff.cuni.cz

Contract/grant sponsor: Ministry of Education of the Czech Republic; contract/grant numbers: MSM 0021620835 and GA AV IAA400550701 (J.V.B, J.E.S.), GAUK-147007 (Z.F.), and AVOZ5004050702 (J.S. and J.E.S.)

interesting features concerning the hypotheses or conclusions made in the experimental works[10,17,20,21,55–59] deserve a more detailed insight based on molecular approach. The $[Ru(\eta^6-arene)(en)Cl]^+$ complexes (en = ethylenediamine, arene = benzene, p-cymen, biphenyl, or derivatives of anthracene) bind to DNA helix in the form of monofunctional adducts (at least in the first step). This is a substantial difference compared with Pt-complexes that primarily form bifunctional adducts with B-DNA. The role of the size of arene ligand was examined experimentally[60] and recently also computational study appeared where the role of base pair - arene stacking was explored.[61] It was found that larger arene ligands like anthracene or biphenyl facilitate complex formation with nucleobases due to π-π stacking interaction. Such interactions are not possible in the case of smaller aromatic molecules with single benzene ring. Also, a pronounced selectivity to guanine was explained[18,60] with formation of an additional H-bond between O6 and the amine group of the ethylenediamine ligand. Such bonding cannot so effectively stabilize neither adenine N7 adduct nor cytosine N3 adduct. However, in the present article it is shown that this is only partially true because some (weaker) H-bond can be formed also in the case of adenine.

The second class of Ru(II) compounds comprises the complexes containing monofunctional pta-ligand (1.3.5-triaza-7-phosphatricyclo[3.3.1.1]decane) (RAPTA class) instead the bifunctional ethylendiamine. Then the Ru cation can coordinate two chloro-ligands and, in this way, some similarities with cisplatin can be expected concerning the mechanism of the drug activity in the cancer cells.

In the present study, we concentrate on the basic quantum chemical characteristics of the first class of Ru(II) "piano-stool" complexes, i.e., those containing an ethylenediamine bidentate ligand. The hydration reaction and adduct formations with guanine, adenine, cytosine, thymine, and uracil are examined from both thermodynamic and kinetic points of view. Also, some physico-chemical characteristics of reactants, products, and transition-state structures were determined for the deeper insight into the reaction course.

Computational Details

In the present study, the compounds of $[Ru(\eta^6-arene)(en)Y]^+$ and $[Ru(\eta^6-arene)(en)X]^{2+}$ (X = H_2O, guanine, adenine, cytosine, thymine, and uracil, Y = Cl^- or OH^-) were examined. Coordination to various interaction sites of nucleobases was explored. Because it is not completely clear, which type of polynucleotides is attacked (single- or double-stranded DNA or RNA), the study was extended to metal interactions with N1, N3, and N7 sites of purine bases and N1 (for completeness), O2, N3, and N4/O4 sites of pyrimidine bases (numbering of atoms in nucleobases is according to standard notation, e.g., Saenger's textbook[62]). The general structure of this class of Ru(II) complexes is drawn in Scheme 1 where pseudo octahedral arrangement of the Ru atom is assumed.

In addition, the aquation and nucleobases replacement processes were considered. In the reaction course, the Cl^- ligand was in the first (activation) reaction replaced by water. As a next reaction, the replacement of the aqua-ligand with purine nucleobase was considered. As arene molecule, benzene (Bz), p-cymene (Cym), biphenyl (Bip) and dihydrogen- and tetrahydrogen-anthracene (DHA and THA, respectively) are used in the first part studying aquation process and benzene and p-cymen in the second part on nucleobase interaction.

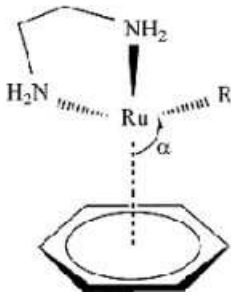

Scheme 1. [Ru(II)(η^6–benzen)(en)R] structure.

To describe the kinetics of the aquation reaction, the supermolecular approach was considered where both reactant molecules (Ru-complex and water) are associated by H-bonding. In the transition state, the formation of '7-coordinated' structure was assumed. Transition states were searched for the replacement of chloro ligand by water in the aquation reaction (activation) and for the subsequent formation of the base adduct in case of the purine nucleobases, guanine and adenine. All the geometries were optimized at the DFT level with the hybrid B3LYP functional and 6-31G(d) basis set - further labeled as B1. The same level was used for the vibration analyses and determination of the ΔG contributions (thermal and entropy terms). The frequency calculations also served for confirmation of the correct character of TS structures as well as reactant and product (super)molecules. The Møller-Plesset second-order perturbation theory MP2/6-31++G(d,p) (basis set labeled as B2 further) was chosen for the single-point (SP) energy determinations and calculations of electronic properties (NBO analyses, dipole moments, and maps of electrostatic and local ionization potentials - not presented here). The Stuttgart-Dresden pseudopotentials[63,64] were chosen for the description of Ru and Cl atoms. The original pseudo-orbitals were extended with a set of polarization functions (with exponents α_f(Ru) = 1.29 and α_d(Cl) = 0.618) for geometry optimizations. The same set of basis functions augmented by diffuse functions (α_s(Ru) = 0.008, α_p(Ru) = 0.011, α_d(Ru) = 0.025, α_s(Cl) = 0.09 and α_p(Cl) = 0.0075) was used for SP calculations. The energy profiles were also reevaluated at the B3LYP/6-31++G(2df,2pd) level (this basis set will be marked as B3). It has been shown that energy barriers of the hydrolysis reaction of cisplatin might be substantially overestimated with double zeta basis sets due to the basis set superposition error.[22] Thus, we have re-calculated the B3LYP energy profiles of the aquation reaction with even larger basis sets, namely aug-cc-pvtz and aug-cc-vpqz. Further, more sophisticated electron correlation calculations were carried out at coupled cluster CCSD/B1 and CCSD/B2 levels. Here, other sets of polarization functions 2fg (α_f = 2.233, 0.6503, α_g = 1.4222) and 2df (α_d = 1.1898, 0.3681, α_f = 0.7062) were optimized for neutral Ru and Cl atoms at CCSD level using steepest descent method

written in MOLPRO 'shell script'. The calculations were performed both in the gas-phase and also in water environment using the Klamt's COSMO implicit solvent approach[65,66] with dielectric constant $\varepsilon = 78$.

Studied complexes are composed from three ligands and a Ru(II) cation and then the total stabilization energy ($\Delta \boldsymbol{E}^{\mathrm{Stab}}$) is defined as:

$$\Delta E^{\mathrm{stab}} = -\left(E_{\mathrm{compl}} - \sum_i E_{\mathrm{Li}} - E_{\mathrm{Ru}} + \Delta E^{\mathrm{deform}} \right). \qquad (1)$$

Here $\boldsymbol{E}_{\mathrm{compl}}$ is total energy of the whole complex, $\boldsymbol{E}_{\mathrm{Li}}$ and $\boldsymbol{E}_{\mathrm{Ru}}$ are BSSE corrected energies of a given ligand $\boldsymbol{i}$ and Ru cation. In this case also the ligand deformation energies were included: $\Delta E^{\mathrm{deform}} = \sum_i (E_{\mathrm{Li}}^{\mathrm{compl}} - E_{\mathrm{Li}}^{\mathrm{opt}})$ where energy terms with superscripts compl and opt denote monomer calculations for the frozen ligand structure taken from the complex (without the ghost functions) and for the optimized isolated ligand, respectively. The ligand bonding and association energies (ΔE^{BE}) were evaluated according to equation:

$$\Delta E^{\mathrm{BE}}(L) = (E_{\mathrm{compl}} - E_{\mathrm{L}} - E_{\mathrm{rest}}). \qquad (2)$$

The $\boldsymbol{E}_{\mathrm{L}}$ and $\boldsymbol{E}_{\mathrm{rest}}$ energies mean the BSSE corrected energy values of the given ligand and the rest of the complex, respectively. No deformation corrections were considered when calculating ΔE^{BE}.

The ground state of all the complexes is a closed-shell singlet. It should be mentioned that in the calculations of BSSE corrections within the COSMO regime, the ghost atomic orbital functions are localized inside the cavity, which has the same size as the whole complex. Then the proper cavitation energy as well as the dispersion and repulsion terms for the solute-solvent interaction has to be taken from other calculations where the actual size of the cavity is considered. We used the $E_{\mathrm{L}}^{\mathrm{compl}}$ values from the calculation of deformation contributions. This is a simpler approach and other possibilities for evaluation of BSSE corrections within the PCM approaches are discussed, e.g., in ref. 67

The kinetic parameters of the studied reactions were determined according to Eyring's Transition State Theory (TST). Because vibrational modes, energies and geometries were obtained from the above described calculations, the rate constants can be estimated from the formula:

$$k^{\mathrm{TST}}(T) = \frac{kT}{\hbar} \cdot \frac{F^{\mathrm{TS}}}{F^{\mathrm{Ru-compl}} F^{\mathrm{w}}} \cdot \exp(E_0/kT). \qquad (3)$$

The F^{X} means molecular partition function per unit volume for the *TS*, *Ru-compl*ex, and *w*ater. E_0 is the activation barrier for the examined reaction coordinate. Determination of $\mathrm{k}^{\mathrm{TST}}$ was performed by the DOIT program kindly provided by Z. Smedarchina.[68] AIM analysis was conducted using Biegler-Koenig AIM2000 program.[69]

Results

Activation of the Ru(II) Complex: Aquation Reaction

In the first part of the study replacement of chloro ligand by water was explored. For optimized complexes of [Ru(arene)(en)Cl]$^+$, [Ru(arene)(en)(OH)]$^+$, and [Ru(arene)(en)(H_2O)]$^{2+}$ the energy analysis and determination of electronic properties were performed. Hydroxo-complex was used for comparison of Ru-O and Ru-Cl dative bonds within the same total charge of the both complexes. Moreover in solution with higher pH values the hydroxo-complex will be preferentially formed. It is clear that neutral aqua ligand posses substantially smaller electrostatic enhancement of the Ru-O dative bond than the $(OH)^-$ anion (or in other words the neutral aqua ligand is a weaker Lewis base). Nevertheless, the dative contribution to the Ru-O interaction should be similar in the both OH^- and water cases.

Table 1. Geometry Parameters of the Isolated Chloro-, Hydroxo-, and Aqua-Complexes at B3LYP/B1 Level of Theory.

		Benzene		p-cymene	
X ligand	Bond [Å]	Gas-phase	COSMO	Gas-phase	COSMO
Cl^-	Ru-N1(en)	2.158	2.144	2.161	2.147
	Ru-N2(en)	2.168	2.151	2.176	2.155
	Ru-Ar	1.720	1.716	1.728	1.728
	Ru-Cl	2.402	2.476	2.411	2.478
OH^-	Ru-N1(en)	2.161	2.148	2.172	2.155
	Ru-N2(en)	2.177	2.157	2.179	2.162
	Ru-Ar	1.715	1.709	1.715	1.715
	Ru-OH	2.019	2.046	2.021	2.049
H_2O	Ru-N1(en)	2.156	2.141	2.163	2.144
	Ru-N2(en)	2.172	2.151	2.179	2.155
	Ru-Ar	1.741	1.718	1.742	1.727
	Ru-H2O	2.236	2.192	2.256	2.203

The distances of the metal—ligand coordination bond in complexes with both benzene and p-cymene are present in Table 1 for gas-phase and COSMO method. The Ru-arene distances (to the center of the aromatic ring) shortens when passing from gas-phase to continuum model, reflecting the hydrophobic character of arene ligands. On the contrary, the coordination bonds of negatively charged Cl^- and OH^- ligands exhibit elongation, which is connected with decreased electrostatic enhancement (which forms a dominant part of their metal—ligand bonding energy). This was observed for coordination distances with neither aqua nor ethylenediamine ligand where a shortening of the Ru-O(aq)/Ru-N(en) bonds can be noticed. In these cases, the explanation can be searched in stronger Ru-O/Ru-N donation as their hydrogen atoms are involved in additional interactions with environment. Confirmation also follows from NBO partial charges and values of bond critical points obtained by AIM analysis. Comparing the coordination distances d(Ru-L) of (en), aqua, OH^- and Cl^- ligands in benzene complexes with analogous distances in cymene complexes, it is clearly seen that all these values are longer in the later case regardless whether gas phase or COSMO calculations are considered. This trend corresponds with the fact that p-cymene is more firmly attached to Ru cation than benzene (cf. below) despite the fact that it is slightly pushed out from metal due to more bulky iso-propyl ligand.

Table 2. MP2/B3 Bonding and Interaction Energies of the Chloro, Hydroxo, and Aqua Ru(II) Complexes (see method for definition).

X ligand	Energy [kcal/mol]	Benzene		p-cymene	
		Gas-phase	COSMO	Gas-phase	COSMO
Cl^-	ΔE^{BE}(*Ru-are*)	−95.1	−94.1	−105.2	−100.7
	ΔE^{BE}(Ru-en)	−105.1	−107.5	−101.0	−105.0
	ΔE^{BE}(Ru-X)	−229.8	−45.8	−221.1	−46.3
	ΔE^{Stab}	591.8	387.4	602.2	393.9
OH^-	ΔE^{BE}(*Ru-are*)	−92.8	−90.0	−102.2	−96.6
	ΔE^{BE}(Ru-en)	−95.0	−93.8	−91.5	−92.5
	ΔE^{BE}(Ru-X)	−268.6	−71.8	−258.9	−71.5
	$\Delta \mathbf{E}^{Stab}$	632.2	415.7	640.3	421.4
H_2O	ΔE^{BE}(*Ru-are*)	−116.3	−101.1	−133.0	−109.2
	ΔE^{BE}(Ru-en)	−134.7	−120.5	−125.7	−118.2
	ΔE^{BE}(Ru-X)	−32.5	−28.6	−29.2	−27.5
	ΔE^{Stab}	395.3	372.7	410.9	377.9

Energy characteristics of these complexes are presented in Table 2. The Table shows that the bonding interactions of arene ligands with metal cation are slightly weaker in comparison with ethylenediamine (in average within 10 kcal/mol). It is interesting to mention that the Ru-arene interaction (cation - π conjugated system) is basically of intramolecular dispersion origin and the bonding energies obtained at the HF level are less than half of MP2 or DFT values. Besides the B3LYP also the BHandH functional (defined as: $0.5*E_X^{HF} + 0.5*E_X^{LSDA} + E_C^{LYP}$) was used for a comparison of the bonding and stabilization energies of the aqua complex in gas phase. The largest difference between B3LYP and BHandH occurred in ΔE^{BE}(Ru-arene) (−95.8 and −125.2 kcal/mol respectively - cf. Table SI 1). Generally, it follows that MP2 and B3LYP calculation give relatively similar bonding energies. The only exception is the Ru-arene interaction where the difference is about 20 kcal/mol and where BHandH functional provides value closer to MP2 result. Better performance of BHandH functional for weak interaction was demonstrated earlier, e.g., by Platts and Robertazzi.[70]

As already mentioned above, both the gas-phase and COSMO calculations display larger bonding energies ΔE^{BE}(Ru-arene) for p-cymene. Because this difference is dominant comparing individual bonding energies of the complexes with both arenes, the total stabilization energies ΔE^{Stab} are also larger for the complexes with cymene. The Ru-X bonding energies (X = water, Cl^-, and OH^-) are the most important in the sense of the possible ligand replacement in a bio-environment. The large bonding energies (in absolute values) of negatively charged species (Cl^- and OH^-) in gas phase are substantially reduced in PCM regime clearly indicating the influence of screening effects, which lead to reduction of the electrostatic contribution to the bonding interactions. Nevertheless, visibly larger bonding energy for oxygen of OH group than for chloride (about 25 kcal/mol in terms of energy) is apparent from Table 2. The bonding energy of electroneutral aqua ligand is only slightly influenced by solvent effects. The solvent polarization mildly increases the electronic density along the Ru-O bond as can be seen from AIM analysis[71] of $[Ru(bz)(en)(H_2O)]^{2+}$ complex in gas phase (density in the Ru-O bond critical point $\rho = 0.049$) and in COSMO approach ($\rho = 0.056$). The same trend can also be observed from increased (in absolute value) partial charges of the Ru, O, N, Cl atoms, which are directly involved in dative interactions. In the case of arene ligand, the lower bonding energies are caused by the decrease of Ru-arene distance (shorter than optimal distances) as a consequence of its hydrophobic character in water solution. The shorter distances shift the system slightly to the repulsive area on the potential energy surface arriving to lower Ru-arene bonding energies. The general trend of lowering energies of dative bonds when passing from gas-phase to continuum model correlates with the analogous trend of the overall stabilization energies.

Interaction of the $[Ru(arene)(en)(H_2O)]^{2+}$ complex with various arene systems were examined at the gas-phase level (presented in Table SI 2). Comparing the optimized geometry parameters, longer Ru-arene distance can be noticed in the chloro-complex with p-cymene where relatively bulky chloro and methyl ligands do not permit closer contact of the aromatic ring with metal cation. Otherwise, no substantial influence of the more extended π-conjugated system can be traced neither in geometry nor in energy characteristics (cf. below). The optimized gas-phase geometries were compared with other computational results[61] and X-ray diffraction measurements.[18] Ru-arene distances are in relatively narrow interval 1.713–1.726 Å, which is in very good agreement with Ru-arene distances from $[Ru(arene)(en)\ (guanine)]^{2+}$ complexes presented by Platts et al.[61] (1.707–1.750 Å) and with experimental results, where slightly shorter values were received (1.66–1.68 Å). On the contrary to all experimental structures, where X-ligand (water or Cl^-) form with long axis of arene an angle ca 25–64°, we found this angle 120–145°, e.g., the structure is oriented reversely - X-ligand stands out of arene and (en) ligand under arene (cf. Fig. 1). In case of biphenyl complexes, similar (33°) propeller torsion angle between both rings was obtained and in anthracene complexes, we found the hinge bending angle on C9–C10 axis about 37° in DHA and ca 20° in THA, which is in reasonable agreement with crystal structures (37 and 11°, respectively).

Kinetics of the Aquation Reaction

The stationary points of the energy profile for the chloro-ligand replacement by water molecule were evaluated. In the supermolecular approach, the geometry changes of the chloro-complex, in comparison with isolated complex from previous part, can be considered as a result of the perturbation due to the interacting water molecule. As a consequence of a large polarization caused by metal cation, this H-bonding interaction is actually not so weak (about 14 kcal/mol in gas-phase). The extent of the perturbation is also apparent from the change of Ru-Cl bond length comparing the corresponding values in Table 1 (for isolated complexes) and Table 3 where the bond lengths in the reactant, TS, and product stage of the reaction are collected for supermolecular model. In gas phase, an elongation of the Ru-Cl distance together with shorter Ru-N1(en) bond points to the place where the water molecule is associated. In COSMO approach, these changes in bond length (correctly) diminish because already

Table 3. Coordination Lengths for Ru(II) Cation in Reactant, TS, and Product Supermolecular Complexes (in Å).

	Reactant		TS		Product	
Distance	Gas-phase	COSMO	Gas-phase	COSMO	Gas-phase	COSMO
Ru-N1(en)	2.151	2.146	2.160	2.137	2.138	2.141
Ru-N2(en)	2.166	2.153	2.182	2.142	2.162	2.143
Ru-bz	1.720	1.713	1.696	1.700	1.721	1.714
Ru-Cl	2.424	2.479	3.099	3.238	3.898	4.271
Ru-H_2O	4.138	4.221	2.586	2.884	2.142	2.168

implicit water affects the geometry of isolated chloro-complex. This can give some qualitative confirmation that the correct trends are obtained in the PCM approaches. In a similar way, Ru-O(aq) and Ru-N1(en) in product supermolecular complex are shortened (in comparison with distances of the corresponding complex in Table 1) under the interaction with Cl^- but also only in the gas-phase calculations. The actual elongation of Ru-O(aq) in product stage in COSMO reflects the situation that water molecule partially follows the chloride particle, which is pulled out into the 'solvent' in comparison with gas-phase results.

Energy profiles of the activation process are collected for selected computational levels in Table 4. The B3LYP/B3 profile is drawn in Figure 2. All the optimized DFT(B3LYP)/B1 structures were subjected to frequency analysis, which confirmed a proper character of all stationary points. In the TS structures, imaginary frequency corresponds to the antisymmetrical stretching mode of O-Ru-Cl atoms. Reaction energy and activation barrier (single point values) were computed at the MP2, CCSD and B3LYP levels with several basis sets (6-31++G(d,p), 6-31++G(2df,2pd), aug-cc-pvtz, and aug-cc-pvqz) both in gas phase and in COSMO regime. A little worse performance of MP2 vs. DFT in comparison to the CCSD(T) method was noticed in the previous study on aquation reaction of cisplatin.[34,72] However, for the Ru(II) complexes the difference between MP2 and B3LYP methods is markedly larger. Therefore, CCSD calculations were performed on DFT optimized structures using two smaller basis sets. MP2 values overestimate the activation barrier and reaction energy in comparison with the both CCSD and experimental results (see below), which match excellently and both are used as reference. The B3LYP results are in better agreement with both reference kinetic data. In addition, the B3LYP activation energies obtained for various double zeta (B1,B2, and B3) bases are close to those obtained with the aug-cc-pvtz and aug-cc-pvqz bases sets. Thus, the activation energies obtained for the aquation of the piano-stool ruthenium complexes do not suffer substantially from the basis set superposition error and can be calculated with an acceptable accuracy using augmented double zeta bases sets (B3LYP/B3). Note, that different behavior was observed for the aquation reaction of cisplatin.[72] The endothermic character of the reaction was obtained (with an exception of DFT/B1 in COSMO approach). In the continuum model at all levels, substantial reduction of activation energy is apparent, thermodynamical results are very close to reference data obtained for larger basis sets. In the last section of Table 4, aquation process for larger arene ligands (Bip, DHA and THA) is present in gas-phase approach and the B3LYP/B3 level. Here, practically no influence of larger aromatic systems on the aquation process can be noticed, similar activation barrier were obtain for all these complexes. This confirm the assumption that larger arenes are mainly important in a later reaction - replacement of water molecule by the nucleobase because the π-π stack interaction can modify the reaction mechanism in real oligomeric DNA/RNA sequences.

Using the B3LYP/B3 level of calculation, the association energies and bonding energies of water and chloride particle in stationary points were determined and are summarized in Table SI 3. It is interesting to notice that in TS, the forming Ru-O bond is still relatively very weak. It increases by only 3 kcal/mol (5 kcal/mol in gas phase) in comparison with the Ru···OH_2 association energy in reactant supermolecule. Similarly, the difference between the Ru-Cl bonding energy in TS and Ru···Cl association energy in product state is about 2 kcal/mol in COSMO model. This indicates that the reaction occurs by facilitated dissociative mechanism. The association/bonding energies were also determined for complexes with other arene ligands with a similar result, e.g., no influence on the (dissociative) reaction mechanism follows from association energies of Cl^- and water determined for complexes with the larger arene ligands.

The calculated thermodynamic and kinetic data can be compared with the experimentally determined aquation process published by Wang et al.[59] where rate constant $k(298)^{forw} = (1.98 \pm 0.02)*10^{-3}$ s^{-1} was obtained. In that article, activation barrier was estimated: $\Delta E_a = 17$ kcal/mol together with the heat of reaction $\Delta H = 2.5$ kcal/mol using DFT method (B3PW91 functional) and COSMO technique. Nevertheless, that barrier is also

Table 4. Estimation of Energy Profile for Chloride Replacement by Water in $\{Ru(bz)(en)Cl\}^+$ Complex (Activation ΔEa and ΔEr Reaction Energies are in kcal/mol, Rate Constants k are in s^{-1}).

	GP				COSMO			
	ΔEa	ΔEr	ΔGr	k	ΔEa	ΔEr	ΔGr	k
MP2/B1	32.5	21.8	21.8	2.3E-12	22.8	3.2	3.2	3.2E-05
MP2/B2	33.1	23.1	23.1	7.7E-13	22.8	6.1	6.0	2.7E-05
MP2/B3					23.9	6.8	6.7	4.5E-06
DFT/B1	27.3	20.7	20.7	1.6E-08	17.2	−1.2	−1.2	3.6E-01
DFT/B2	27.9	22.1	22.0	5.0E-09	18.5	1.9	1.8	4.2E-02
DFT/B3	28.8	23.6	23.6	1.1E-09	19.2	2.8	2.8	1.4E-02
DFT/aug-cc-pvtz					19.1	2.9	2.9	1.5E-02
DFT/aug-cc-pvqz					19.1	2.9	2.9	1.5E-02
CCSD/B1					20.8	1.7	1.6	9.3E-04
CCSD/B2					20.9	4.5	4.4	7.6E-04
DFT/B3	28.7	18.3	20.0	1.3E-09		p-Cymen		
	29.2	18.5	18.3	0.6E-09		Biphenyl		
	29.3	19.1	19.0	0.5E-09		2H-Antracene		
	28.5	18.2	17.5	2.0E-09		4H-Antracene		

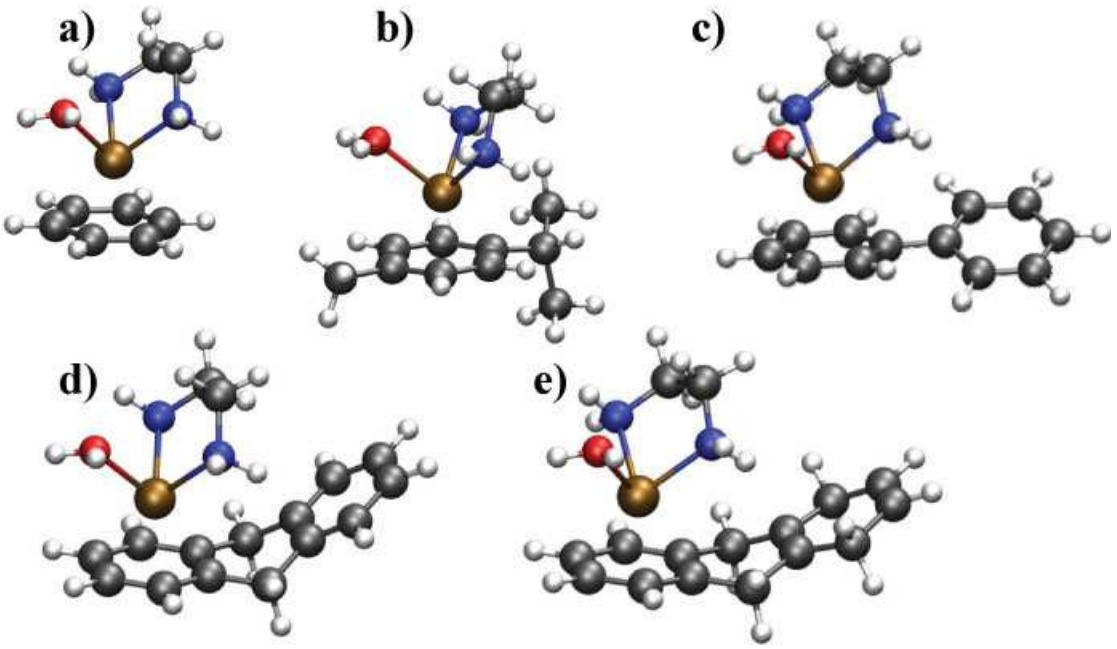

Figure 1. $[Ru(arene)(H_2O)(en)]^+$ complexes where arene ligand is: a) benzene, b) p-cymene, c) biphenyl, d) dihydrogen-anthracene, e) tetrahydrogen-anthracene.

partially underestimated because the measured rate constant corresponds to barrier height ca 21 kcal/mol. Using Eyring's formula from the TST theory, the rate constant of the replacement process is estimated from optimized geometries and (unscaled) frequence calculations at the B3LYP/B1 level in combination with the energy profile determined at several computational levels. In this way, the rate constant of the pseudo-first order forward reaction is estimated: $k(298)^{forw} = 1.5*10^{-2}$ s^{-1} and backward reaction has a rate constant $k(298)^{backw} = 1.3$ s^{-1} M^{-1}. For the 37°C, the following values were obtained:

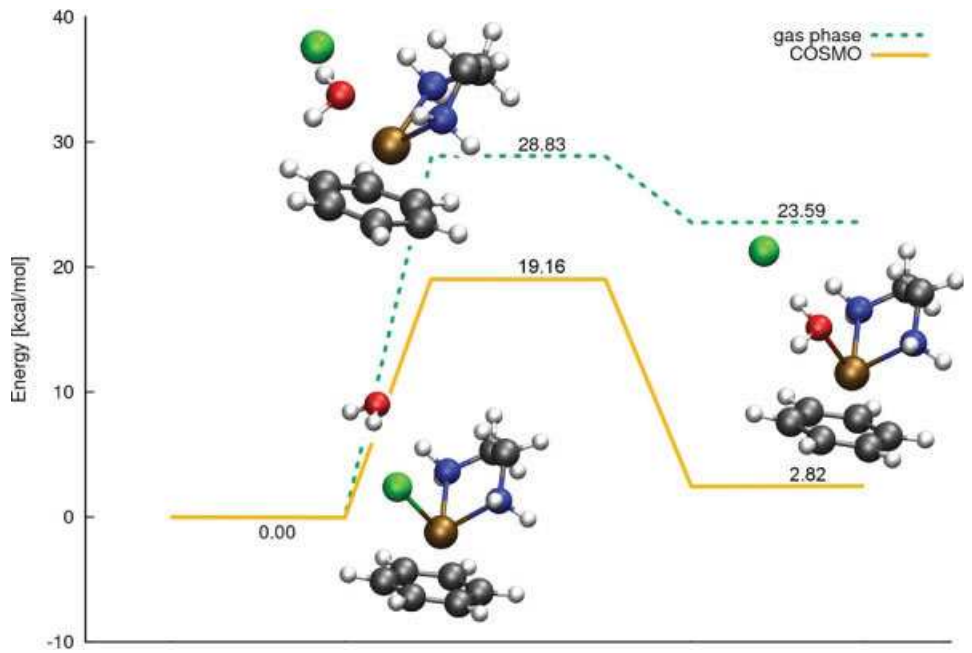

Figure 2. ΔE energy profile (at the B3LYP/B3 level) of the aquation reaction for $[Ru(bz)(en)Cl]^+$ complex. Solid line in gas phase. dashed line in COSMO.

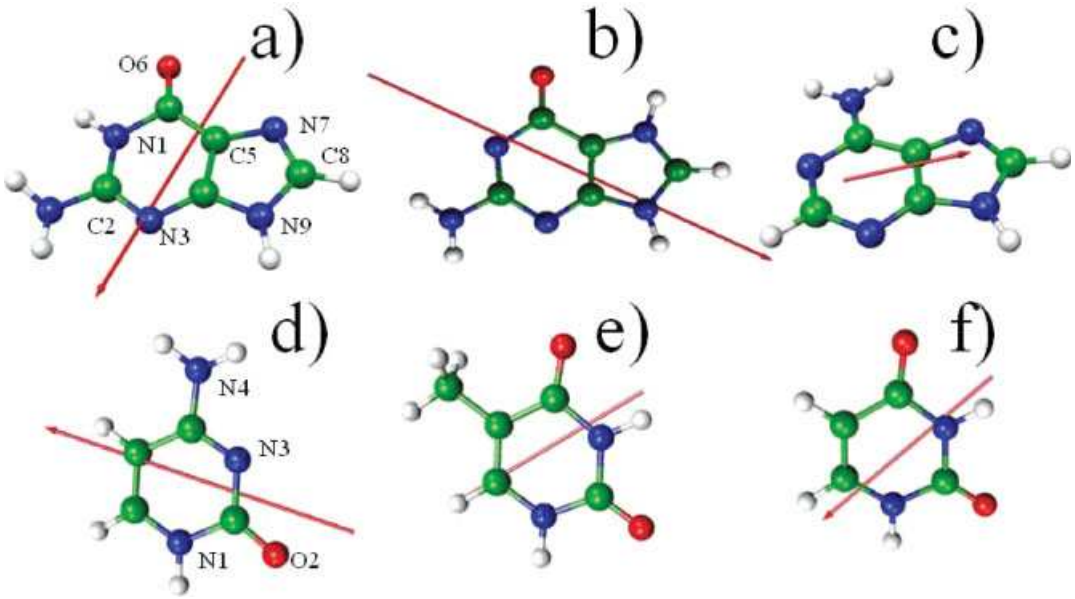

Figure 3. Orientation and size of the dipole moments of isolated NA bases calculated in gas phase at the MP2/B3 level. a) guanine b) N7 protonated guanine c) adenine d) cytosine, e) thymine, f) uracil.

$k(310)^{forw} = 6.1*10^{-2}$ s^{-1} and $k(310)^{backw} = 3.9$ s^{-1} M^{-1}. These results can be compared directly with above mentioned experimental value[59] determined by UV-VIS spectrometry. The difference of one order of magnitude reflects the energy difference of ca 2 kcal/mol in the height of activation barrier, which can be considered within an error bar of the energy calculations (considering the levels of method - B3LYP, pseudopotentials, PCM, and basis set). The CCSD/B2 activation barrier leads to very accurate estimation of rate constant $k(298) = 8*10^{-4}$ s^{-1}. Based on the achieved results, the B3LYP/B3 level can be suggested as sufficiently accurate for calculations of larger systems. The DFT approach underestimates the CCSD results by 1–2 kcal/mol, whereas the MP2 method with the same basis set overestimates both energies by about 2–3 kcal/mol. Because aquation rate constants for other arene molecules (p-cymene, biphenyl, DHA and THA) are available from experimental study,[18] gas-phase estimation was performed for comparison. Obtained rate constants are collected in last section of Table 6. Despite great discrepancy in absolute values between calculated and measured rate constants, relative values show practically no influence of the arene π-conjugated system on the rate of aquation. Analogous conclusion also follows from studies of Sadler group (refs. 18,59) where the variation of rate constants between (1.28 and 2.36)$*10^{-3}$ s^{-1} was found.

Interaction of Ru(II) Complexes With Nucleobases

In the second part of the study, the interactions of the piano-stool Ru(II) complexes with both purine and pyrimidine nucleobases is examined, the structures and their dipole moments are displayed in Figure 3. In the case of guanine and adenine, energy profiles for the replacement reaction of aqua-ligand by the base were also determined.

Ru(II) Adducts With Various Sites of Nucleobases

Structures. In the first part, adducts of ruthenium complexes to various interacting sites of guanine and adenine were explored. Bonding energies for conformers with Ru(II) cation interacting with N1, N3, (O6 in guanine), and N7 nucleobase positions were compared in the complexes with the benzene ligand. Only the most stable conformers in the PCM regime (N7 adducts) were chosen for the examination of bonding properties in the complexes with p-cymene. Basic coordination parameters of these structures are summarized in Table SI 4.

For adenine, the shortest Ru-N(A) distance occurs in a complex where N3 site interacts with metal cation. In this structure, a relatively short Ru-N3 distance occurs (2.140 Å) together with short (repulsive) H···H contact between N9-H···H-N2(en) sites (2.292 Å). It results in elongated Ru-N2(en) bond (2.182 Å), the longest Ru-N(en) bond within all the cases explored in the study. In this way, the donation of the N2(en) to metal cation is reduced giving additional space for competitive coordination of the adenine N3 site. The consequence of this coordination relationship can be also found in bonding energies resulting in the lowest $\Delta \boldsymbol{E}^{BE}$(en) (in absolute value) from all the explored systems. In water environment, these effects are attenuated because the five-member ring moves from the H-N2(en) by about 0.14 Å. Nevertheless, the Ru-N3(A) coordination still remains the shortest among all the Ru-N(Base) distances despite the fact that this is the only complex where the Ru-N bond length was increased when passing from the gas phase to COSMO approach (see Table SI 4a). In the case of Ru-N7(A) complex, the Ru-N7 bond length is 2.16 Å and a weaker H-bond interaction between N6···H-N(en) can be noticed with the N···H distance 1.96 Å (cf Fig. 4).

In the case of N1 adduct of guanine, the tautomer with hydrogen transferred to the N7 site is considered in the further

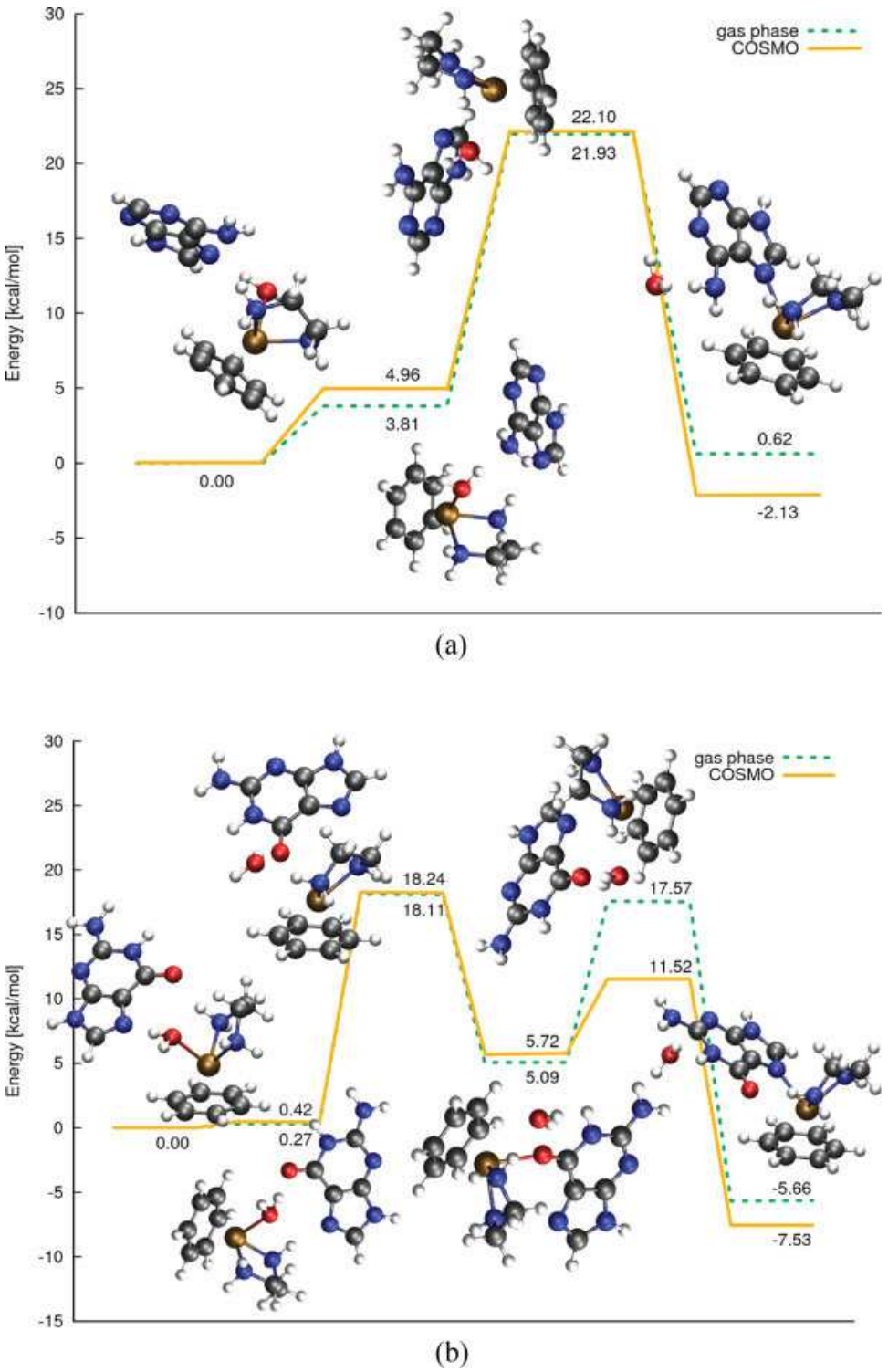

Figure 4. ΔE energy profiles (at the B3LYP/B3 level) of aqua substitution by a) adenine and b) guanine. [Color figure can be viewed in the online issue, which is available at www.interscience.wiley.com.].

analyses. The possibility of the proton transfer to O6 was also examined but it is energetically less stable (e.g., by about 6 kcal/mol in COSMO). In the case of guanine conformers, the shortest Ru-N(G) distance occurs in the N7-adduct. It can be noticed that coordination distances resemble corresponding geometry parameters of the N7-adenine complex. However, the relatively short Ru-N2(en) bond is apparent, which is linked with a strong O6···H-N2(en) H-bonding (1.756 Å). The same picture occurs in the cymene complex, too. Interestingly, Ru-N3(G) adduct does not exhibit so markedly short Ru-N3 bond and elongated Ru-N2(en) bond, because the H···H repulsion is diminished here. From the interatomic distances, it can be noticed that distance between $N9^{\delta-}\cdots H^{\delta+}$-N2(en) is shorter than (G)N9-H···H-N2(en), which is not the case of the Ru-N3(A) complex. Finally, the Ru-O6(G) adduct was explored. The Ru-O6 distance is relatively short in correspondence with orientation of the guanine dipole moment but still longer than the corresponding Ru-N7 coordination in Ru-N7(G) adduct. Also the H-bonding interaction between N7···H-N2(en) atoms is not so strong (1.872 Å).

The interactions of metal complexes with all three pyrimidine nucleobases were explored, too. In these complexes, only the structures with benzene ligand were considered. Note that the N1 pyrimidine positions are in nucleic acids occupied by the attached sugars, so these positions cannot be utilized for ion binding in nucleic acids. Note also that when the cation binds to N(H) nucleobase positions, the corresponding proton is moved to some acceptor site of the nucleobase, leading to a different tautomeric form. Optimized distances of Ru(II) dative bonds are placed in Table SI 4b.

The ruthenium adducts with N1, N3, and O2 cytosine sites were considered. In the Ru-N1(C) adduct, proton from the N1 site was transferred to another heteroatom; protonation of the N3 position was found energetically more stable than the O2 position, similarly to the Ru-N1(G) conformer where N7 site was preferred over O6. Complexes coordinated to N4 atom were also considered but the structures with proton transferred to either O2 or N3 positions were substantially less stable. It was found that the shortest Ru-X(C) coordination (X = N1, N3, and O2) occurs in the Ru-O2 conformer. This conformer was also found the most stable in gas-phase calculations, which is slightly surprising when we realize that this is the only nucleobase where the oxygen position is preferred for metal coordination over nitrogen sites. In the COSMO regime, the Ru-O2 distance still remains the shortest from all the considered Ru-X distances, however, the stabilization energy preference is inverted and both the Ru-N1 and Ru-N3 adducts are more stable. This demonstrates the influence of electrostatic effects because relatively large cytosine dipole moment (μ = 6.55 D at MP2/B2 level) is oriented in the C2–C5 direction (cf. Fig. 3). It is interesting to notice that also the Ru-arene and Ru-N(en) distances attain the shortest values in the same Ru-O2(C) complex in both gas phase and COSMO approaches. This shows that oxygen σ-dative ability is not so strong (more probably) or it is compensated by π back-donation, leaving some additional space for donation of the other ligands. The later assumption is not confirmed by MO analysis (no MO with combination of occupied d(Ru) AOs and virtual antibonding MO of cytosine was found) nevertheless, second-order perturbation theory energies within the NBO analysis give some support for possible back-donation.

In ruthenium complexes with thymine and uracil, the geometry relationships are similar to the situation in cytosine adducts. The Ru-X coordination bonds are shorter in the Ru-O adducts, especially in the Ru-O4 complex (in both thymine and uracil). On the contrary to the Ru-O2(C) adduct, no Ru-O complex (with neither thymine nor uracil) represents the most stable conformation not even in gas phase (cf. discussion on energy part below). It is also worth to mention that the Ru-N1 adducts of both bases prefer conformations with proton transferred to O2 (the N3 site is already occupied by another hydrogen). In the case of Ru-N3(T,U) adducts, the more stable conformations have proton transferred to O4 position.

Energy Analysis

The bonding, stabilization, and total energies (where relevant) for the most stable conformers are displayed in Table 5. In the case of purine bases, the most stable structures differ for adenine and guanine bases in the gas-phase calculations. Although the Ru-N1(A) conformer is preferred in the adenine complexes, the Ru-N7(G) conformer has the lowest total electronic and stabilization energies among the guanine structures. Nevertheless in the COSMO regime, the N7-conformer represents the most stable form for the both nucleobases. This change of preference match with the general concept according to that the influence of electrostatic forces is decreased (screened) in PCM approaches. In gas phase, the Ru-N1(A) coordination is visibly enhanced by favorable orientation of the adenine dipole moment μ = 2.70 D (determined at the MP2/B2 gas-phase level) in N1–C8 direction whereas in guanine the dipole is oriented in N7–N3 direction, μ = 6.36 D as can be seen in Figure 3. Even larger dipole moment oriented in N1–C8 direction occurs in N1-guanine tautomer (μ = 9.55 D). This dipole is responsible for the fact that the Ru-N1(G) adduct exhibits the highest ΔE^{BE}(Ru-N(base)) bonding energy from all the explored complexes (both in gas phase and COSMO levels). The same effect (reduction of electrostatic enhancement) causes the change in energy preference in the cytosine adducts. Passing from gas phase to the implicit solvent, the Ru-O2(C) structure becomes the least stable by more than 7 kcal/mol and the most stable adduct is Ru-N1(C). The Ru-N3(C) complex has practically the same stabilization and total electronic energies; the differences are within 1 kcal/mol. Uracil and thymine identically prefer the N3 coordination regardless the environment. This preference is in accord with different orientation of the dipole moment of uracil and thymine in comparison with cytosine (cf. Fig. 3). All the remaining conformers (even the Ru-N1(T,U)) have substantially smaller stabilization energies.

Because the replacing of various ligands of the ruthenium complexes are explored in the study, it is important to know how strongly metal cation interacts with individual ligands. Therefore, bonding energies were evaluated. Comparing individual systems, the Ru-en interaction energies are around ca 120 kcal/mol in water surrounding. The ΔE^{BE}(*Ru-arene*) energies are preserved in the range of 100–110 kcal/mol for benzene and 110–120 kcal/mol for cymene in gas-phase calculations. Water

Table 5. Bonding and Stabilization Energies at the MP2/B2 level (in kcal/mol); for Comparison of Various Adducts also Total Energies (in a.u.) are Presented.

	Ru(bz)(N1-ade)		Ru(bz)(N3-ade)		Ru(bz)(N7-ade)		Ru(cym)(N7-ade)	
Adenine	*gas phase*	COSMO	*gas phase*	COSMO	*gas phase*	COSMO	*gas phase*	COSMO
ΔE^{BE}*(are)*	−105.4	−100.2	−105.3	−99.5	−104.6	−100.1	−119.9	−108.7
ΔE^{BE}*(en)*	−129.0	−122.3	−125.8	−121.4	−131.3	−123.3	−124.2	−121.4
ΔE^{BE}*(ade)*	−72.7	−48.7	−69.1	−47.7	−69.7	−50.3	−65.4	−50.2
ΔE^{Stab}	431.1	389.2	426.9	387.9	426.2	390.0	441.4	396.5
E^{Total}+900	−81.612	−81.880	−81.605	−81.879	−81.606	−81.881		
Guanine	Ru(bz)(N1-gua)		Ru(bz)(N3-gua)		Ru(bz)(N7-gua)		Ru(cym)(N7-gua)	
ΔE^{BE}*(are)*	−101.3	−96.0	−107.0	−104.4	−102.9	−95.3	−117.6	−103.8
ΔE^{BE}*(en)*	−125.4	−118.4	−132.6	−124.8	−129.6	−122.3	−122.2	−117.8
ΔE^{BE}*(gua)*	−103.9	−59.7	−56.4	−45.3	−90.7	−56.0	−86.1	−57.2
ΔE^{Stab}	442.7	390.9	412.6	384.7	449.7	395.3	465.6	383.3
E^{Total}+1000	−56.687	−56.944	−56.637	−56.939	−56.695	−56.955		
Cytosine	Ru(bz)(N1-cyt)		Ru(bz)(N3-cyt)		Ru(bz)(O2-cyt)			
ΔE^{BE}*(are)*	−101.4	−94.9	−105.7	−98.2	−103.7	−95.4		
ΔE^{BE}*(en)*	−126.5	−117.6	−128.2	−120.1	−122.7	−115.0		
ΔE^{BE}*(cyt)*	−89.5	−56.0	−79.0	−52.8	−84.0	−45.9		
ΔE^{Stab}	441.1	392.6	438.4	392.2	444.6	389.2		
E^{Total}+900	−9.447	−9.710	−9.444	−9.709	−9.449	−9.701		
Thymine	Ru(bz)(N1-thy)		Ru(bz)(N3-thy)		Ru(bz)(O2-thy)		Ru(bz)(O4-thy)	
ΔE^{BE}*(are)*	−105.5	−97.6	−103.5	−96.1	−109.9	−103.0	−109.8	−102.4
ΔE^{BE}*(en)*	−125.3	−119.9	−125.7	−117.7	−124.3	−116.9	−125.6	−117.6
ΔE^{BE}*(thy)*	−65.0	−46.5	−82.8	−51.3	−53.9	−31.3	−60.0	−34.7
ΔE^{Stab}	407.4	372.3	424.9	380.3	412.5	374.0	420.2	376.2
E^{Total}+900	−68.436	−68.717	−68.467	−68.727	−68.440	−68.717	−68.454	−68.721
Uracil	Ru(bz)(N1-ura)		Ru(bz)(N3-ura)		Ru(bz)(O2-ura)		Ru(cym)(O4-ura)	
ΔE^{BE}*(are)*	−106.3	−98.0	−103.8	−95.8	−110.4	−103.0	−110.0	−102.2
ΔE^{BE}*(en)*	−125.8	−120.3	−126.2	−118.1	−126.2	−118.5	−126.0	−118.0
ΔE^{BE}*(ura)*	−61.6	−45.9	−79.8	−51.1	−50.8	−31.7	−59.1	−34.3
ΔE^{Stab}	403.2	371.2	422.7	380.5	410.5	375.3	419.3	377.3
E^{Total}+900	−29.240	−29.527	−29.274	−29.539	−29.247	−29.531	−29.262	−29.534

solution decreases these values by about 5–10 kcal/mol. For the singly bonded ligands (nucleobases), substantially larger bonding energy reduction occurs, when passing from vacuo to water solution. The strongest coordination bonds are formed in guanine complexes, where ΔE^{BE}*(Ru-N(G))* is up to 100 kcal/mol in gas phase, which is comparable with ΔE^{BE} of the 'triply' bonded benzene molecule. In the case of implicit water environment the bonding energies of guanine drop to ca 60 kcal/mol. These energies are in good accord with the similar studies both experimental[73,74] and computational[24,42,49] on transition metal interactions with nucleobases. The cytosine bonding energies are also relatively high, around 80 kcal/mol in gas phase. Slightly weaker Ru-N dative bonds are formed in complexes with thymine and uracil, and the lowest energies were found for adenine coordination, about 70 kcal/mol. In the COSMO regime, the same order of bonding energies can be seen. However, the ΔE^{BE}*(Ru-N(base))* values are in much narrower range (from 50 to 60 kcal/mol). Most of these values are close to 50 kcal/mol, which is actually the same energy which was obtained for platinum interaction in electroneutral adenine and guanine complexes.[75,76] This value can be considered as an upper limit for the pure coordination energy of the Ru(II)-N(base) dative bond (without electrostatic contribution) in analogy to Pt(II)-N(base) bonds.[75]

Activation Barriers and Kinetics for Water-Nucleobase Exchange Process

In analogy to aquation-dechlorination reaction, the replacement of the aqua ligand by purine nucleobase was investigated using the supermolecular approach. The supermolecular model is suitable approach when exploring the kinetics of some reaction - for the determination of an activation barrier. On the other hand using this approach does not consider the association energy and/or association Gibbs free energy. Although the former one is nearly always negative (individual species usually attract each other), in the case of association Gibbs free energy, this is not always valid due to the different distribution of the degrees of freedom (separated species has each three translational and rotational degrees of freedom), which has important consequences in determination of the entropy term. For a more realistic estimation of the reaction rate, the probability factor for formation of the associated reactant complex (or in other words its real con-

Table 6. Energy Profile of the Aqua-Ligand Replacement by Purine Nucleobase From $[Ru(bz)(en)(H_2O)]^{2+}$ Complex (activation ΔEa, ΔEr, and ΔGr reaction energies are in kcal/mol, rate constants in M^{-1} s^{-1}).

	GP							COSMO						
Guanine	Δ*E*a1	Δ*E*r1	Δ*G*r1	Δ*E*a2	Δ*E*r2	Δ*G*r2	*k*(1)	Δ*E*a1	Δ*E*r1	Δ*G*r1	Δ*E*a2	Δ*E*r2	Δ*G*r2	*k*(1)
MP2/B1								17.1	3.2	1.6	4.5	−13.9	−11.6	1.7E+00
MP2/B2	19.5	0.1	−1.5	15.5	−15.5	−13.2	3.4E-02	14.8	1.5	−0.1	3.1	−15.3	−13.0	8.2E+01
MP2/B3								16.1	2.4	0.7	2.1	−15.5	−13.2	1.0E+01
DFT/B1	19.8	5.5	3.9	15.4	−9.3	−7.0	1.9E-02	18.8	6.3	4.7	8.0	−11.5	−9.3	1.1E-01
DFT/B2								17.7	5.9	3.8	6.0	−13.6	−11.4	7.0E-01
DFT/B3	17.8	5.1	3.5	12.5	−10.8	−8.5	5.2E-01	17.8	5.7	3.7	5.8	−13.3	−11.0	5.4E-01
Adenine														
MP2/B1								20.6	−3.4	−4.2				5.0E-03
MP2/B2	24.3	−8.5	−9.3				9.9E-06	17.5	−7.0	−7.9				8.7E-01
MP2/B3								17.7	−6.2	−7.0				6.4E-01
DFT/B1	24.3	3.5	2.7				9.0E-06	19.6	1.0	0.2				2.8E-02
DFT/B2								17.3	−2.0	−2.8				1.3E+00
DFT/B3	18.1	0.6	−4.0				3.2E-01	17.1	−2.1	−2.9				1.7E+00

centration) should be taken into account together with a value of the rate constant.

The arrangement of molecules in reactant complex, TS, and product state was optimized. Hessian matrix of second derivatives was diagonalized confirming proper character of the obtained structures. In the transition state, one negative vibration mode corresponding to O(aq)-Ru-N7(B) antisymmetric stretch was found. Key coordination parameters (lengths of dative Ru-L bonds) are summarized in Table SI 5. In the case of adenine, the global supermolecular minimum on the reactant side (with two H-bonds: (A)N7···H—O(aq) and (A)N6···H-N(en)) of the potential energy surface (PES) does not correspond to the appropriate initial arrangement for the explored reaction coordinate. The correct reaction minimum structure has to have opposite orientation of adenine: (A)N7···H-N(en) and (A)N6···H-O(aq). This conformer lies about 5 kcal/mol higher on the PES (B3LYP/B3) in COSMO approach, cf. Figure 4a. Although the water-adenine exchange reaction passes through simple reaction mechanism, in the case of guanine no single TS reaction coordinate was found. Instead, two-step reaction mechanism is suggested. The reaction minimum of the first step has the analogous arrangement as the adenine local (reaction) minimum. The reaction minimum lies only slightly higher (less than 1 kcal/mol) than global supermolecular minimum as it can be noticed in Figure 4b. Result of the first step (an intermediate) is a complex with guanine coordinated through O6 site (about 6 kcal/mol above global supermolecular reaction minimum). This structure is subsequently change to more stable N7 adduct passing very low second transition barrier with a character of metastable chelate O6-Ru-N7. The final Ru-N7 product lies about 5–8 kcal/mol lower than reactant complex.

Such a metal-O6 coordination was not found for platinum complexes in our previous studies because Pt(II) cation has weaker affinity (by about 25 kcal/mol) for O6 atom than N7. In the case of corresponding Ru(II) structures the analogous difference in total energy is only 9 kcal/mol). This results partially contradicts to study of Borgoo et al.[77] According to their results the Ru atom is slightly softer than Pt so that Ru affinity to harder oxygen should be lower than the affinity of the Pt atom according to the Pearson HSAB principle.[78]

Energy profiles of the exchange reaction are compiled in Table 6 and Figure 4. On the basis of DFT(B3LYP)/B3 level, it was determined that replacement of aqua ligand by both adenine and guanine is an exothermic process. In the guanine replacement process, slightly larger reaction heat is released (about 8 kcal/mol). The first reaction step is by about 6 kcal/mol endothermic and is also a rate controlling process with the activation barrier of ca 18 kcal/mol. The height of the subsequent barrier is about 6 kcal/mol. According to the obtained rate constants (at the DFT/B3 level), the formation of adenine adduct (k(A) = 1.7 M^{-1} s^{-1}) should be three times faster than in the case of guanine (k(G) = 0.54 M^{-1} s^{-1}) if the same concentration of both nucleobases is assumed. However, it should be taken into account that in the case of adenine the reaction minimum lies relatively high above global minimum. Thus, the occurrence of the reaction minimum is very low according to Boltzmann equilibrium distribution law (about $2.3*10^{-04}$), which influences the actual reaction rate for adenine replacement substantially (the process follows second order reaction kinetics). In the guanine case, the ratio for occurrence of reaction/global minima is 0.49. Moreover, rate constants from the MP2/B3 level (a little bit less accurate according to Table 4) suggest opposite kinetic preference (k(G) = 10 vs. k(A) = 0.64 M^{-1} s^{-1}). As followed from Table 6, the exchange reaction for both nucleobases has lower activation barriers than in the case of aquation reaction.

It can be concluded that in real DNA/RNA, guanine adducts will prevail approaching the thermodynamic equilibrium- complexes with guanine should represent 95% occurrence of all adducts (assuming only guanine and adenine can form adducts).

For the verification of the facilitated dissociative mechanism, the $\Delta \boldsymbol{E}^{\mathrm{BE}}$ association/bonding energies for water and nucleobases are evaluated (cf. Table SI 6). It was found that adenine is really very weakly coordinated in the TS structure, which gives sufficient support for facilitated dissociative mechanism. In the case guanine, some dative bonds character seems to already exist in the TS1 structure where the base interacts by additional

6 kcal/mol. Comparing the $\Delta E^{BE}(Ru\text{-}X(G))$ bonding energies of intermediate and product, close values like for isolated Ru-O6(G)/Ru-N7(G) adducts were obtained (42.3/56.0 kcal/mol).

Moreover, from the Table SI 6 the association free Gibbs energies of guanine and adenine with hydrated ruthenium complex can be noticed. These values clearly demonstrate that the reactant complex will not be formed spontaneously. Hydration of both reactant molecules is more preferable process. From the comparison of the guanine and adenine association Gibbs energies, it follows that the reactant complex with guanine will be formed with substantially higher probability than in the case of adenine. The population of guanine reactants is about 1000 times higher than adenine one considering the energy difference of ca 4 kcal/mol and the room temperature. Because this reaction is governed by the second order kinetics, the concentration of the reactants directly influence the reaction rate. In this way, the smaller rate constant for guanine replacement is overweighed by substantially higher concentration of the guanine reactant complex.

Conclusions

In this study, the piano-stool $[Ru(II)(\eta^6\text{-arene})(en)Y]^+$ and $[Ru(\eta^6-arene)(en)X]^{2+}$ complexes (X = H_2O, guanine, adenine, cytosine, thymine, and uracil, Y = Cl^- or OH^-) were explored using advanced quantum chemical methods. All these structures were optimized at DFT(B3LYP)/B1 level and single point properties were determined at the MP2/B3 level. The aquation process (replacement of chloro ligand by water) and exchange reaction of aqua ligand by nucleobases were examined at several level of ab initio and DFT theories (MP2, CCSD and B3LYP) and several basis sets ranging from medium-polarized 6-31G(d) to extended aug-cc-pvqz one. Environment effects were included using polarizable continuum model with the COSMO method. The calculations reveal that the solvent screening is of primary importance for the studied complexes.

For adenine, the N1-adduct is more stable than the N7-conformer in the gas phase. However, when solvent effects are considered the N7-conformer becomes more stable due to effective screening of the electrostatic contributions. Similar result is obtained for cytosine where the Ru-O2 adduct is the most stable *in vacuo* but the least stable (from the explored cytosine conformers) in polar solvent.

The thermodynamic and kinetic data were determined for aquation process and compared with available experimental studies. There is an excellent agreement between experiment and theory at the CCSD level and an acceptable accord in the case of the B3LYP/B3 approximation. Although DFT underestimates both reaction energy and the height of the activation barrier, MP2 method overestimates them.

Exchange reaction was studied for both purine bases. It was found that local minimum, which is about 4–5 kcal/mol above the global supermolecular minimum structure, is involved in determination of reaction coordinate in the complexes with adenine (Fig. 4a). In the guanine case this simple reaction mechanism does not exist. Instead, two-step reaction mechanism is suggested where first the Ru-O6(G) coordination is formed, which is subsequently transformed through chelate TS to the most stable Ru-N7(G) conformer.

Comparing thermodynamic and kinetic parameters for both bases, it was ascertained that formation of the ruthenium complex with guanine is slightly slower. Because the "concentration" of the appropriate adenine-Ru(are)(en)H_2O supermolecular conformer will be very low, faster reaction course can be actually expected in guanine exchange reaction. The guanine adduct will definitely dominate in the real DNA/RNA sequences according to the both thermodynamic and kinetic criteria.

The present article brings thorough QM characterization of molecular interactions in the studied systems and key reference structures can be found in Supporting Information.

Acknowledgments

The computational resources from Meta-Centrum Project (in Prague, Plzen, and Brno) as well as computational cluster of Faculty of Mathematics and Physics are acknowledged for access to their excellent computational facilities.

References

1. Caruso, F.; Rossi, M. Mini Rev Med Chem 2004, 4, 49.
2. Uudsemaa, M.; Tamm, T. Chem Phys Lett 2001, 342, 667.
3. zu Berstenhorst, B. M.; Erker, G.; Kehr, G.; Wasilke, J. C.; Muller, J.; Redlich, H.; Pyplo-Schnieders, J. Eur J Inorg Chem 2005, 92.
4. Korfel, A.; Scheulen, M. E.; Schmoll, H.-J.; Gruendel, O.; Harstrick, A.; Knoche, M.; Fels, L. M.; Skorzec, M.; Bach, F.; Baumgart, J.; Safi, G.; Seeber, S.; Thiel, E.; E., B. W. Clin Cancer Res 1998, 4, 2701.
5. Asara, J. M.; Hess, J. S.; Lozada, E.; Dunbar, K. R.; Allison, J. J Am Chem Soc 2000, 122, 8.
6. Katsaros, N.; Anagnostopoulou, A. Crit Rev Oncol Hematol 2002, 42, 297.
7. Sorasaenee, K.; Galan-Mascaros, J. R.; Dunbar, K. R. Inorg Chem 2002, 41, 433.
8. Rubin, J. R.; Haromy, T. P.; Sundaralingam, M. Acta Crystallogr Sect C 1991, 47, 1712.
9. Goodgame, D. M. L.; Omahoney, C. A.; Page, C. J.; Williams, D. J. Inorg Chim Acta 1990, 175, 141.
10. Chen, H.; Parkinson, J. A.; Parsons, S.; Coxal, R. A.; Gould, R. O.; Sadler, P. J Am Chem Soc 2002, 124, 3064.
11. Gisselfaelt, K.; Lincoln, P.; Norden, B.; Jonsson, M. J Phys Chem B 2000, 104, 3651.
12. Hartmann, M.; Robert, A.; Duarte, V.; Keppler, B. K.; Meunier, B. J Biol Inorg Chem 1997, 2, 427.
13. Kueng, A.; Pieper, T.; Wissiack, R.; Rosenberg, E.; Keppler, B. K. J Biol Inorg Chem 2001, 6, 292.
14. Lincoln, P.; Norden, B. J Phys Chem B 1998, 102, 9583.
15. Liu, J.-G.; Ye, B.-H.; Zhang, Q.-L.; Zou, X.-H.; Zhen, Q.-X.; Tian, X.; Ji, L. -N. J Biol Inorg Chem 2000, 5, 119.
16. Malina, J.; Novakova, O.; Keppler, B. K.; Alessio, E.; Brabec, V. J Biol Inorg Chem 2001, 6, 435.
17. Novakova, O.; Chen, H.; Vrana, O.; Rodger, A.; Sadler, P. J.; Brabec, V. Biochemistry 2003, 42, 11544.
18. Wang, F.; Chen, H. M.; Parsons, S.; Oswald, L. D. H.; Davidson, J. E.; Sadler, P. J. Chem Eur J 2003, 9, 5810.
19. Vaidyanathan, V. G.; Nair, B. U. J Inorg Biochem 2002, 91, 405.
20. Serli, B.; Zangrando, E.; Gianferrara, T.; Scolaro, C.; Dyson, P. J.; Bergamo, A.; Alessio, E. Eur J Inorg Chem 2005, 3423.
21. Peacock, A. F. A.; Habtemariam, A.; Fernandez, R.; Walland, V.; Fabbiani, F. P. A.; Parsons, S.; Aird, R. E.; Jodrell, D. I.; Sadler, P. J. J Am Chem Soc 2006, 128, 1739.

22. Dorcier, A.; Dyson, P. J.; Gossens, C.; Rothlisberger, U.; Scopelliti, R.; Tavernelli, I. Organometallics 2005, 24, 2114.
23. Lau, J. K. C.; Deubel, D. V. J Chem Theory Comput 2006, 2, 103.
24. Lau, J. K. C.; Deubel, D. V. Chem Eur J 2005, 11, 2849.
25. Deubel, D. V. J Am Chem Soc 2006, 128, 1654.
26. Wysokinski, R.; Michalska, D. J Comput Chem 2001, 22, 901.
27. Pavankumar, P. N.; Seetharamulu, P.; Yao, S.; Saxe, J. D.; Reddy, D. G.; Hausheer, F. H. J Comput Chem 1999, 20, 365.
28. Dos Santos, H. F.; Marcial, B. L.; De Miranda, C. F.; Costa, L. A. S.; De Almeida, W. B. J Inorg Biochem 2006, 100, 1594.
29. Costa, L. A. S.; Rocha, W. R.; De Almeida, W. B.; Dos Santos, H. F. J Inorg Biochem 2005, 99, 575.
30. Raber, J.; Zhu, C.; Eriksson, L. A. J Phys Chem 2005, 109, 11006.
31. Robertazzi, A.; Platts, J. A. J Comput Chem 2004, 25, 1060.
32. Zhang, Y.; Guo, Z.; You, X.-Z. J Am Chem Soc 2001, 123, 9378.
33. Burda, J. V.; Zeizinger, M.; Leszczynski, J. J Comput Chem 2005, 26, 907.
34. Burda, J. V.; Zeizinger, M.; Leszczynski, J. J Chem Phys 2004, 120, 1253.
35. Zeizinger, M.; Burda, J. V.; Šponer, J.; Kapsa, V.; Leszczynski, J. J Phys Chem A, 2001, 105, 8086.
36. Lopes, J. F.; Menezes, V. S. D.; Duarte, H. A.; Rocha, W. R.; De Almeida, W. B.; Dos Santos, H. F. J Physical Chem B 2006, 110, 12047.
37. Šponer, J. E.; Leszczynski, J.; Šponer, J. J Phys Chem B 2006, 110, 19632.
38. Burda, J. V.; Leszczynski, J. Inorg Chem 2003, 42, 7162.
39. Zeizinger, M.; Burda, J. V.; Leszczynski, J. Phys Chem Chem Phys 2004, 6, 3585.
40. Baik, M.-H.; Friesner, R. A.; Lippard, S. J. J Am Chem Soc 2002, 124, 4495.
41. Baik, M. H.; Friesner, R. A.; Lippard, S. J. Inorg Chem 2003, 42, 8615.
42. Baik, M. H.; Friesner, R. A.; Lippard, S. J. J Am Chem Soc 2003, 125, 14082.
43. Eriksson, M.; Leijon, M.; Hiort, C.; Norden, B.; Graeslund, A. Biochemistry 1994, 33, 5031.
44. Coll, M.; Sherman, S. E.; Gibson, D.; Lippard, S. J.; Wang, A. H.-J. J Biomol Structure Dyn 1990, 8, 315.
45. Spiegel, K.; Rothlisberger, U.; Carloni, P. J Phys Chem B 2004, 108, 2699.
46. Robertazzi, A.; Platts, J. A. Inorg Chem 2005, 44, 267.
47. Schroeder, G.; Kozelka, J.; Sabat, M.; Fouchet, M.-H.; Beyerle-Pfnur, R.; Lippert, B. Inorg Chem 1996, 35, 1647.
48. Chval, Z.; Šíp, M. J Mol Struct 2000, 532, 59.
49. Pavelka, M.; Burda, J. V. J Mol Model 2006, 13, 367.
50. Deubel, D. V. J Am Chem Soc 2004, 126, 5999.
51. Zimmermann, T.; Zeizinger, M.; Burda, J. V. J Inorg Biochem 2005, 99, 2184.
52. Broo, A.; Lincoln, P. Inorg Chem 1997, 36, 2544.
53. Gossens, C.; Tavernelli, I.; Rothlisberger, U. Chimia 2005, 59, 81.
54. Deubel, D. V.; Lau, J. K. C. Chem Commun 2006, 2451.
55. Aird, R.; Cummings, J.; Ritchie, A.; Muir, M.; Morris, R.; Chen, H.; Sadler, P.; Jodrell, D. Br J Cancer 2002, 86, 1652.
56. Berners-Price, S. J.; Ronconi, L.; Sadler, P. J. Prog Nucl Magn Reson Spectrosc 2006, 49, 65.
57. Kašparková, J.; Mackay, F. S.; Brabec, V.; Sadler, P. J. J Biol Inorg Chem 2003, 8, 741.
58. Habtemariam, A.; Melchart, M.; Fernandez, R.; Parsons, S.; Oswald, I. D. H.; Parkin, A.; Fabbiani, F. P. A.; Davidson, J. E.; Dawson, A.; Aird, R. E.; Jodrell, D. I.; Sadler, P. J. J Med Chem 2006, 49, 6858.
59. Wang, F. Y.; Habtemariam, A.; van der Geer, E. P. L.; Fernandez, R.; Melchart, M.; Deeth, R. J.; Aird, R.; Guichard, S.; Fabbiani, F. P. A.; Lozano-Casal, P.; Oswald, I. D. H.; Jodrell, D. I.; Parsons, S.; Sadler, P. J. Proc Natl Acad Sci USA 2005, 102, 18269.
60. Chen, H. M.; Parkinson, J. A.; Moris, R. E.; Sadler, P. J. J Am Chem Soc 2003, 125, 173.
61. Gkionis, K.; Platts, J. A.; Hill, J. G. Inorg Chem 2008, 3893.
62. Saenger, W. Principles of Nucleic Acid Structure; Springer-Verlag: New York, 1983.
63. Andrae, D.; Haussermann, U.; Dolg, M.; Stoll, H.; Preuss, H. Theor Chim Acta 1990, 77, 123.
64. Bergner, A.; Dolg, M.; Kuechle, W.; Stoll, H.; Preuss, H. Mol Phys 1993, 80, 1431.
65. Klamt, A. J Phys Chem 1995, 99, 2224.
66. Klamt, A.; Schüürmann, G. J. Chem Soc, Perkin Trans 1993, 2, 799.
67. Pavelka, M.; Burda, J. V. J Phys Chem A 2007, submitted.
68. Smedarchina, Z.; Fernández-Ramos, A.; Siebrand, W. J Comput Chem 2001, 22, 787.
69. Biegler-Koenig, F.; Schoenbohm, J., AIM2000 version 2.0, 2002.
70. Robertazzi, A.; Platts, J. A. Chem Eur J 2006, 12, 5747.
71. Bader, R. F. W. Atoms in Molecules: A Quantum Theory; Oxford Univ. Press: Oxford, 1990.
72. Burda, J. V.; Zeizinger, M.; Leszczynski, J. J Comput Chem 2005, 29, 907.
73. Marzilli, L. G.; Ano, S. O.; Intini, F. P.; Natile, G. J Am Chem Soc 1999, 121, 9133.
74. Reedijk, J. Chem Rev 1999, 99, 2499.
75. Burda, J. V.; Šponer, J.; Leszczynski, J. J Biol Inorg Chem 2000, 5, 178.
76. Burda, J. V.; Šponer, J.; Leszczynski, J. Phys Chem Chem Phys 2001, 3, 4404.
77. Borgoo, A.; Torrent-Sucarrat, M.; De Proft, F.; Geerlings, P. J Chem Phys 2007, 126, 234104.
78. Parr, R. G.; Pearson, R. G. J Am Chem Soc 1983, 105, 7512.

Comparison of hydration reactions for "piano-stool" RAPTA-B and [Ru(η^6– arene)(en)Cl]$^+$ complexes: Density functional theory computational study

Zdeněk Chval,[1] Zdeněk Futera,[2] and Jaroslav V. Burda[2,a)]
[1]*Department of Laboratory Methods and Medical Technology, Faculty of Health and Social Studies, University of South Bohemia, J. Boreckého 27, 370 11 České Budějovice, Czech Republic*
[2]*Department of Chemical Physics and Optics, Faculty of Mathematics and Physics, Charles University, Ke Karlovu 3, 121 16 Prague 2, Czech Republic*

(Received 10 June 2010; accepted 22 October 2010; published online 12 January 2011)

The hydration process for two Ru(II) representative half-sandwich complexes: Ru(arene)(pta)Cl_2 (from the RAPTA family) and [Ru(arene)(en)Cl]$^+$ (further labeled as Ru_en) were compared with analogous reaction of cisplatin. In the study, quantum chemical methods were employed. All the complexes were optimized at the B3LYP/6-31G(d) level using Conductor Polarizable Continuum Model (CPCM) solvent continuum model and single-point (SP) energy calculations and determination of electronic properties were performed at the B3LYP/6-311++G(2df,2pd)/CPCM level. It was found that the hydration model works fairly well for the replacement of the first chloride by water where an acceptable agreement for both Gibbs free energies and rate constants was obtained. However, in the second hydration step worse agreement of the experimental and calculated values was achieved. In agreement with experimental values, the rate constants for the first step can be ordered as RAPTA-B > Ru_en > cisplatin. The rate constants correlate well with binding energies (BEs) of the Pt/Ru–Cl bond in the reactant complexes. Substitution reactions on Ru_en and cisplatin complexes proceed only via pseudoassociative (associative interchange) mechanism. On the other hand in the case of RAPTA there is also possible a competitive dissociation mechanism with metastable penta-coordinated intermediate. The first hydration step is slightly endothermic for all three complexes by 3–5 kcal/mol. Estimated BEs confirm that the benzene ligand is relatively weakly bonded assuming the fact that it occupies three coordination positions of the Ru(II) cation. © *2011 American Institute of Physics*. [doi:10.1063/1.3515534]

I. INTRODUCTION

Despite cisplatin is a very effective anticancer metallodrug, an intensive research of some other metallocomplexes is carried out. The reason is based on the fact that cisplatin is very toxic with many side effects.[1] Another problem consists in low or even no activity for some kinds of carcinomas.[2] Therefore many studies appeared on complexes, which are active against cancer cells. Various biophysical and biochemical properties of rhodium,[3–7] titanium,[8–10] ruthenium,[11–24] and many other metal complexes[25,26] were explored.

Computational studies usually concentrate on coordination and structural effects. Description of the reaction mechanisms and electronic properties of cisplatin and its analogs were examined in several papers.[27–31] Some studies concerned the aquation process of platinum complexes, which is crucial in the activation step,[32–39] interactions with nucleobases,[40–51] or other competitive reactions with cellular components, such as side chains of amino acids.[52–56]

Ruthenium compounds also attract a lot of attention as can be noticed in recent computational chemistry literature.[19,57–64] A lot of interesting features, hypotheses and conclusions, which would be worth of computational confirmations or deserve a more detailed insight based on molecular modeling can be found in many experimental works.[18,21,24,25,65–72] An interesting paper on stacking interaction of Ru(II) complexes with guanine and adenine using density functional theory (DFT) study was presented by Platts.[73]

There are two basic families of half-sandwich ruthenium(II) complexes. First class (further labeled as Ru_en) is represented by [Ru(η^6−arene)(en)Cl]$^+$ complexes[67,74] (en = ethylenediamine, arene = benzene), which can coordinate to DNA helix in the form of monofunctional adducts (at least in the first step). This is one of the basic differences compared to Pt-complexes where bifunctional adducts are believed to be the key structure coordinated to the genomic sequence. The role of the size of the arene ligand was examined, too.[17] It was found that larger arene ligands like anthracene or biphenyl increase the drug efficiency due to possible intercalation into DNA helix via $\pi-\pi$ stacking interaction. This interaction is reduced in the case of smaller aromatic ligands with a single benzene ring. Also, a pronounced selectivity (higher affinity) of these Ru(II) complexes to guanine was discussed in Refs. 17 and 19. The explanation was searched in a formation of an additional H-bond between O6 and the amine group of the ethylenediamine ligand. Such a strong binding can be created neither with N7-adenine nor with N3-cytosine adduct. However, in our previous paper it was shown[75] that this is only

a)Author to whom correspondence should be addressed. Electronic mail: burda@karlov.mff.cuni.cz. Tel.: +420 221 911 246. Fax: +420 221 911 249.

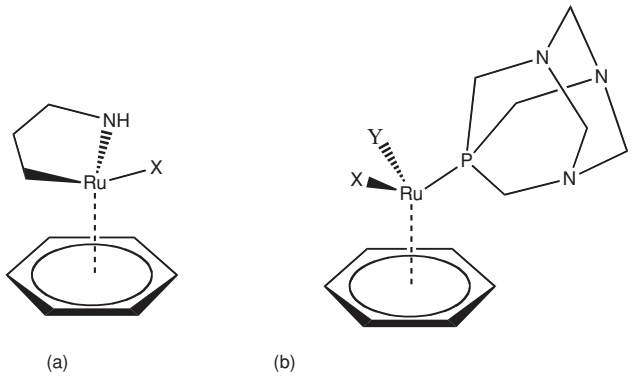

SCHEME 1. Structural formulas of (a) Ru_en and (b) RAPTA-B complexes.

partially true since some (weaker) H-bond can be formed also in the case of adenine. We confirmed that the size of arene ring does not play any role in the activation reaction so that the extent of aromatic system does not substantially change the coordination strength of the Ru-arene part of the complex.[75] Also, the H-bonding between ethylenediamine and exocyclic N6 amino group of adenine is markedly weaker than analogous interaction in the guanine complex (at least according to N6...H/O6...H distance which is 2.07 and 1.83 Å, respectively) or according to electron density of the bond critical points obtained from Bader's Atoms-in-Molecules (AIM) analysis.[76]

The second class of the Ru(II) "piano-stool" compounds examined in this study is the so-called RAPTA family. We used a model complex RAPTA-B (further called just RAPTA), which contain monofunctional pta ligand (1.3.5-triaza-7-phosphatricyclo[3.3.1.1]decane),[77,78] benzene, and two chloride anions. In this way, some similarities with cisplatin can be expected concerning the mechanism of the drug activity in the cancer cells.

The general structures of both Ru(II) classes are drawn in Scheme 1.

In the present study we compare activation process, e.g., hydration reactions of basic representatives of both classes of half-sandwich ruthenium complexes together with the frequently studied cisplatin complex. The DFT computational level and the CPCM continuum solvent model were employed for determination of all explored structures in reactants, products and transition states. Besides energy profiles, also some physicochemical and electronic characteristics were determined for the deeper insight into the reaction mechanism.

II. COMPUTATIONAL DETAILS

In the present study, the compounds of $[Ru(\eta^6-arene)(en)X]^{+/2+}$ and $[Ru(\eta^6-arene)(pta)XY]^{0/1+/2+}$ (X, Y = Cl^-, OH, H_2O) were examined. The general structures of both classes of Ru(II) complexes contain the pseudo-octahedral arrangement of the Ru atom. For the comparison cisplatin hydration is also included.

All the explored systems were optimized both in the gas phase and in water environment using the Klamt's COSMO (CPCM) implicit solvent approach[79,80] with dielectric constant $\varepsilon = 78$. In chosen model, default Klamt's cavities were used.

In the reaction course of the pseudoassociative mechanism (PAM), the Cl^- ligand(s) was/were replaced by water. In order to describe the reaction kinetics of the hydration reactions, the supermolecular approach was considered. In the reactant state, the Ru-complexes and water are associated by H-bonding. The transition states for the replacement of chloro ligand by water were found where formation of a seven-coordinated structure was revealed. In the Ru_en complexes, only one step is possible while activation of the RAPTA and cisplatin complexes can occur in two subsequent steps replacing both chloride ligands. Moreover in the RAPTA complex also a dissociative mechanism was explored where two reaction steps in each dechloration were determined. The first TS structure is linked with Ru–Cl bond breaking. Then the five-coordinated intermediate is formed with both chloride and water particles detached from the RAPTA complex. Finally, the second TS complex follows where oxygen of water is approaching and forming a new coordination bond.

All the geometries were optimized at the DFT level with the hybrid B3LYP functional and 6-31G(d) basis set (further labeled as BS1) with the description of heavy elements Pt, Ru, P, and Cl atoms by Stuttgart energy averaged pseudopotentials.[81,82] The original pseudo-orbital basis set was extended by polarization functions (with exponents $\boldsymbol{\alpha}_f$(Pt) = 0.98, $\boldsymbol{\alpha}_f$(Ru) = 1.29, $\boldsymbol{\alpha}_d$(P) = 0.51, and $\boldsymbol{\alpha}_d$(Cl) = 0.62) in the optimization part. The same level was used for the determination of the ΔG contributions (thermal and entropy terms) and also for confirmation of the proper character of the optimized geometries of TS structures as well as reactant and product supermolecules in both gas phase and CPCM approach. The energy profiles were determined at the B3LYP/6–311++G(2df,2pd)/CPCM level (BS2) expression where original pseudo-orbitals of metals were consistently augmented by a set of diffuse and polarization (2fg) functions optimized for neutral atoms at CCSD level, as mentioned elsewhere.[75,83]

As it can be noticed from Scheme 1 the complexes are composed from three/four ligands and the metal cation. The total stabilization energy (ΔE^{Stab}) of the complex is defined as

$$\Delta E^{\mathrm{Stab}} = -\left(E_{\mathrm{compl}} - \sum_{\mathrm{i}}^{\mathrm{Ligands}} E_{\mathrm{i}} - E_{\mathrm{Me}} + \Delta E^{\mathrm{deform}}\right). \quad (1)$$

Here E_{compl} is total energy of the whole complex, E_i and E_{Me} are BSSE corrected energies of a given ligand i and Me—the metal cation. In this case, the ligand deformation energies were included

$$\Delta E^{\mathrm{deform}} = \sum_{\mathrm{i}}^{\mathrm{Ligands}} \left(E_{\mathrm{i}}^{\mathrm{compl}} - E_{\mathrm{i}}^{\mathrm{opt}}\right). \quad (2)$$

In the equation the superscripts compl and opt denote calculations for the frozen ligand structure (taken from geometry of the complex) and for the optimized (isolated) ligand, respectively. The ligand binding and/or association energies (ΔE^{BE}) were evaluated according to equation

$$\Delta E^{\mathrm{BE}}(L) = (E_{\mathrm{compl}} - E_{\mathrm{L}} - E_{\mathrm{rest}}). \quad (3)$$

TABLE I. Metal-ligand coordination distances (in Å) within the hydration reactions for $[Ru(arene)(en)Cl]^+$, $[Ru(arene)(pta)Cl_2]$, and $[Pt(NH_3)_2Cl_2]$ complexes. The optimized bond lengths were obtained at the B3LYP/BS1/CPCM and T = 298 K level.

		Ru–Cl	Ru–Ben	Ru–N1	Ru–N2	Ru–O
Ru_en_Cl+w		2.479	1.713	2.146	2.151	4.218
TS_en		3.238	1.700	2.137	2.142	2.883
Ru_en_w+Cl		4.288	1.714	2.143	2.143	2.166
	Ru–Cl	Ru–Cl	Ru–Ben	Ru–P	Ru–O	Ru–O
Ru_pta_Cl2+w	2.473	2.477	1.740	2.343	3.810	
TS_pta1a	2.447	3.305	1.716	2.359	2.918	
TS_pta1d1	2.397	3.698	1.714	2.362	4.391	
Int1	2.380	5.244	1.717	2.365	4.794	
TS_pta1d2	2.358	4.960	1.711	2.382	3.584	
Ru_pta_Cl_w+Cl	2.448	4.375	1.741	2.348	2.159	
Ru_pta_Cl_w+w	2.458		1.743	2.347	2.175	4.070
TS_pta2a	3.206		1.715	2.367	2.199	2.724
TS_pta2d1	3.598		1.714	2.376	2.153	3.862
Int2	6.970		1.738	2.375	1.945	4.468
TS_pta2d2	5.137		1.703	2.398	2.16	3.461
Ru_pta_w2+Cl	4.207		1.740	2.362	2.176	2.148
Ru_pta_Cl_OH+w	2.496		1.763	2.335	2.087	
TS_pta2d1+OH	6.970		1.738	2.375	1.945	4.468
Int2_OH	4.397		1.711	2.387	1.957	3.090
TS_pta2d2_OH	4.477		1.734	2.352	2.064	2.18
Ru_pta_OH_w+Cl	2.496		1.763	2.335	2.087	
	Pt–Cl	Pt–Cl	Pt–N	Pt–N	Pt–O	Pt–O
Pt_a2_Cl2+w	2.361	2.363	2.066	2.065	3.862	
TS_cis1	2.354	2.798	2.058	2.045	2.467	
Pt_a2_Cl_w+Cl	2.349	4.083	2.070	2.034	2.082	
Pt_a2_Cl_w+w	2.360		2.068	2.074	2.021	3.738
TS_cis2	2.908		2.043	2.031	2.119	2.653
Pt_a2_2w+Cl	4.016		2.045	2.045	2.107	2.107
Pt_a2_Cl_OH+w	2.357		2.083	2.039	2.102	3.768
TS_cis2_OH	3.009		2.057	2.094	2.004	2.405
Pt_a2_OH_w+Cl	4.103		2.087	2.026	2.005	2.086

Similarly, the E_L and E_{rest} energies mean the BSSE corrected values of the given ligand and the remaining part of the complex, respectively. In these energies, deformation corrections were not considered.

The ground state of all the explored complexes is a closed-shell singlet. In the calculations of BSSE corrections within the CPCM regime, the ghost atomic orbital functions are localized inside the cavity, which has the same size as the whole complex. This is the simplest approach and discussion on other possibilities for determination of BSSE corrections within the PCM model can be found in Ref. 55.

The kinetic parameters of the studied reactions were determined according to Eyring's transition state theory. Because vibration modes, energies, and geometries are available from the above-described calculations, the rate constants can be estimated from the formula

$$k(T) = (k_B T/h)\, \exp(-\Delta G^{\neq}/RT). \quad (4)$$

The calculations of electronic properties [Natural Bond Orbital (NBO) and AIM analyses, and dipole moments] were performed at the same computational level as SP calculations (B3LYP/BS2). AIM analysis was performed by AIMALL program of T. Keith[84] and natural population analysis (NPA) partial charges were determined by NBO v.5 program from University of Wisconsin.[85]

A. Structures

All structures of the stationary points on the reaction profiles of the hydration reactions were optimized in both gas phase and CPCM levels. The obtained metal-ligand distances in water environment are collected in Table I. Longer distances between the metal and the arene ring can be noticed in the case of the RAPTA complexes compared to the Ru_en complexes due to higher steric crowding. The Ru–P bond of the pta ligand is about 2.34 Å in neutral reactant and it slightly increases with total charge of the complex up to 2.36 Å in the diaqua product. It means that origin of this bond is basically nonelectrostatic. In the product states of the both classes of Ru complexes, Ru–O distance (≈2.17 Å) is visibly longer than analogous Pt–O coordination bonds in cisplatin. The same is also true for the Ru–N bonds in Ru–en complexes and Ru–Cl bonds in Ru–pta reactants. All these distances are about 0.1 Å shorter in the Pt(II) complexes. The simplest possible explanation follows from a general study on covalent radii published recently[86] where the difference of covalent radii of Pt and Ru atoms is about

0.1 Å. The binding energy unambiguously correlates with electron density of the bond critical point, as it will be discussed below.

Transition states of Ru(II) piano-stool complexes in the 'pseudoassociative mechanism' are represented by the hepta-coordinated structures where one can easily expect relatively large sterical repulsion. However the exchanging ligands are practically nonbonded (see the part on binding energies below) in TSs so that lower binding competition occurs and visibly shorter Ru–arene distances can be noticed (in comparison with both reactant and product states). This effect is a little bit more pronounced in PCM geometries than in gas phase. Similar shortening is observed for the Ru–N coordination distances of the ethylenediamine ligand in TS of the Ru–en complex (TS_en) and for the equatorial amino ligands in the trigonal-bipyramidal TSs structures of cisplatin. On the contrary, in the case of the RAPTA TS structures, the Ru–P bond of the pta ligand is elongated. Similarly the Ru–O distance of the aqua ligand in second reaction step elongates in TS geometry (TS_pta2a) where the Ru–O bond is about 2.199 Å (despite of H-bonding between both water molecules and chloride) and in second hydration step (TS_cis2) where the axial Pt–N bond is also elongated (2.094 Å). The shortening can be explained by a lower competition to Pt–N bond in equatorial plane of trigonal-bipyramid due to very weakly bounded exchanging ligands. On the contrary, the coordination of the axial ligands is generally known to be always a little bit longer (and weaker).

Another reaction mechanism was revealed in the case of RAPTA complexes. The competitive dissociation mechanism is linked with two TS structures and one metastable penta-coordinated intermediate in each dechloration reaction. This intermediate has the two pta and Cl/aqua/hydroxo ligands oriented in a plane perpendicular to the arene ring. Such an arrangement minimizes the interligand repulsion. In this way it is obvious why this direct dissociative mechanism (dDM) could not occur in the Ru_en complex. The ethylenediamine bidentate ligand cannot form similar kind of structure (where en ligand would be perpendicular to arene ring) due to high-energy penalty caused by deviation of the donating electron lone-pairs of nitrogens from the ideal sp^3 orientation and by increased arene…H(en) steric repulsion. Basically all the structural trends from the discussion on TS of pseudoassociative mechanism are also valid for geometries of the intermediates and TS's of the dissociative pathway.

B. Energy profile of hydration reactions

All the energy characteristics of the explored complexes are summarized in Table II and corresponding reaction energy profiles are drawn in Fig. 1 for PAM and in Fig. 2 for dDM. In the first reaction step of PAM, all the explored reactions are endoergic with $\Delta G_r \approx 3$–6 kcal/mol and have comparable activation barrier of about 20 kcal/mol for the replacement of the first chloride.

In the second reaction step of the RAPTA and cisplatin complexes, much higher activation energy (over 25 kcal/mol) was determined for pseudoassociative mechanism together with more pronounced endoergic reaction course of about 8–11 kcal/mol. This feature can be explained by the fact that in the monoaqua reactant the remaining chloro ligand is more strongly bond as follows from higher binding energy of the Ru–Cl in Table III (compare BE of 52 kcal/mol for monochloro reactant in the second hydration step with BE of 42 kcal/mol for dichloro-reactant in the first step). The same conclusion also follows from Table IV where the AIM critical points are displayed [corresponding Bond Critical Point (BCP) values of Ru–Cl are 0.065 versus 0.062 *e*/a.u.[3] (Ref. 3)].

The higher extent of similarity between the RAPTA complex and cisplatin follows not only from a structural factor but

TABLE II. Gibbs energy reaction surface (in kcal/mol) and rate constants (in s^{-1} in gray) at the B3LYP/BS2/CPCM level.

	Calc.	Expt.
Ru_en_Cl+w	0.00	
TS_en	20.01	
Ru_en_w+Cl	2.79	
	1.32E-02	(1.98 ± 0.02) E-03[a]
Ru_pta_Cl2+w	0.00	
TS_pta1_a	18.95	
Ru_pta_Cl_w+Cl	3.31	
	7.98E-02	(3.33 ± 0.02) E-03[b]
Ru_pta_Cl2+w	0.00	
TS_pta1_d1	18.72	
Int_1	18.46	
TS_pta1_d2	20.59	
Ru_pta_Cl_w+Cl	4.12	
	4.72E-03[d]	
Ru_pta_Cl_w+w	0.00	
TS_pta2a	26.49	
Ru_pta_w2+Cl	10.83	
	2.37E-07	(5.5 ± 0.2) E-02[b]
Ru_pta_Cl_w+w	0.00	
TS_pta2_d1_w	19.90	
Int2_w	17.90	
TS_pta2_d2_w	27.98	
Ru_pta_2w+Cl	6.23	
	1.87E-08[d]	
Ru_pta_Cl_OH+w	0.00	
TS_pta2_d1_OH	11.88	
Int2_OH	6.96	
TS_pta2_d2_OH	12.56	
Ru_pta_OH_w+Cl	4.58	
	2.90E+03[d]	
Pt_a2_Cl2+w	0.00	
TS_cis1	23.86	
Pt_a2_Cl_w+Cl	5.24	
	1.99E-05	(1.9 ± 0.2)E-04[c]
Pt_a2_Cl_w+w	0.00	
TS_cis2	28.95	
Pt_a2_2w+Cl	10.99	
	3.73E-09	
Pt_a2_Cl_OH+w	0.00	
TS_cis2	25.90	
Pt_a2_OH_w+Cl	10.51	
	6.94E-07	(2.3 ± 0.3)E-04[c]

[a]Reference 19.
[b]Reference 88.
[c]Reference 89.
[d]$k_1k_2(k_1 + k_2)$ for subsequent reversible reactions.

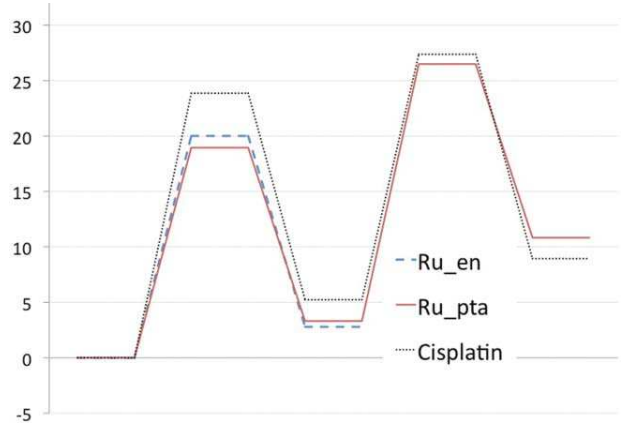

FIG. 1. Energy profile of pseudoassociative hydration reactions of $[Ru(arene)(en)Cl]^+$, $[Ru(arene)(pta)Cl_2]$, and $[Pt(NH_3)_2Cl_2]$ complexes at the B3LYP/6–31++G(2dp,2pd)/CPCM(UA0) level.

also from the shape of the reaction energy profile. In the case of cisplatin, the activation barrier of the first step is a little higher than in RAPTA (23 vs 19 kcal/mol) but otherwise the shape is more or less the same (energy of all the other stationary points on the reaction coordinate differs at most by 2 kcal/mol). However, one should keep in mind that the similarity deals only with the hydration reaction and (probably) does not concern the subsequent reactions since the role of arene ligand is believed to be important in stacking interactions with nucleobases in genomic code. This aspect was not considered in the study and it is not fully enlightened even *in vitro* and *in vivo* experiments at present. Our previous calculations[75] on this topic as well as results from other groups[57,87] seem to confirm this assumption.

In the neutral or basic solutions the hydroxo ligand should be considered instead of the aqua ligand (for cisplatin the experimental pK_a is 5.5; calculated value ≈6.2 (Ref. 54) and analogous calculations for Ru_pta_wCl complex lead to estimation of ca 7.7 (Ref. 19). This leads to lower activation barrier (by about 3 kcal/mol) due to higher competition of negatively charged OH group in comparison with neutral aqua ligand. Moreover, in the case of RAPTA_OH complex the second dechloration step cannot occur within the PAM mechanism. Instead, the direct dissociation mechanism was found with two lower reaction barriers (≈12 and 6 kcal/mol). The

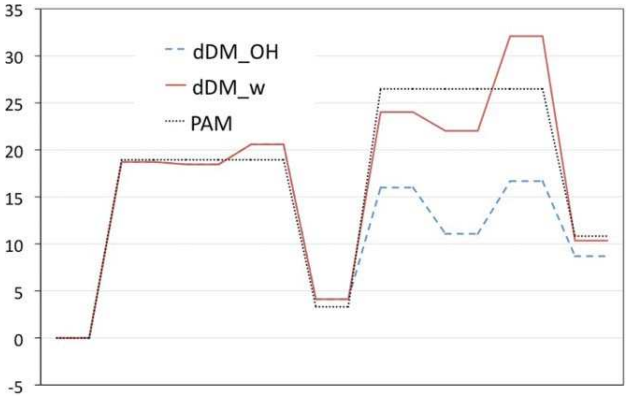

FIG. 2. Reaction coordinate for the dissociative mechanism of RAPTA dechlorination at the B3LYP/6-31++G(2dp,2pd)/CPCM level.

same dissociation mechanism was also determined for hydrated RAPTA complex in presence of aqua ligand. Here, the activation barriers were found 19 and 10 kcal/mol. It means that lower reaction barrier was also confirmed for dissociation mechanism in acidic and neutral solutions. The dDM pathway has practically the same activation energy for the first dechloration reaction as PAM ($\Delta G_a^1 \approx 19$ kcal/mol). No dDM was found in cisplatin hydration.

C. Binding energies

Table III summarizes the stabilization and binding energies evaluated according to Eqs. (1) and (3), respectively. Two different kinds of stabilization energies are present. Besides standard definition (ΔE^{Stab}) based on Eq. (1) the other energy (ΔE^{Stex}) represents total coordination energy of the metal cation with the ligands fixed in their optimal positions in the given complex. The ΔE^{Stex} energy is determined according to Eq. (3) supposing E_L is energy of the metal cation and E_{rest} represents the frozen structure of all the ligands. In this way, mutual repulsion of the ligands is not included from the obtained value and this repulsion basically forms the main difference between both ΔE^{Stab} and ΔE^{Stex} values (besides deformation correction involved in ΔE^{Stab} value). As to deformation energies, it can be seen that the smallest values were obtained in the case of cisplatin where smallest number of ligands (small molecules—water and ammonia) is present. The largest deformations are in the Ru_en complexes mainly due to deformation of the en-ligand (about 5 kcal/mol). The deformation of the benzene ligand is ≈3 kcal/mol in the both Ru complexes. The repulsion energy of the ligands (as a $E^{Stab} - E^{Stex}$ difference) clearly shows the highest values in cisplatin complexes where values up to 30 kcal/mol can be seen. Substantially smaller values were gained in the RAPTA complexes and the smallest repulsion was determined in the Ru_en complexes since only one negatively charged ligand is present there.

Comparing the metal-am(m)ino binding energies, it can be noticed that the en ligand is slightly less coordinated in the Ru_en complex than ammines in cisplatin. Confirmation of this fact can be observed from a comparison of BCP in Table IV where all the densities in BCP of Pt-N(H_3) are higher than 0.1 e a.u.$^{-3}$ while the Ru-N(en) densities are always lower than this value. The BE of benzene is slightly higher in the Ru_en complex than in RAPTA which is in accord with the larger number of BCP's of the Ru–C bonds in the Ru_en complexes. In this case also smaller partial charge of Ru(II) cation of the RAPTA complexes (cf. Table V) can be responsible for the lower electrostatic cation—π system contribution. In these complexes it can be noticed that the pta ligand is coordinated with similar BE as both chloride ligands. Electrostatic enhancement of Ru–Cl bond is compensated by a larger coordination character of the Ru–P bond as follows from BCP analysis. The Ru–P bond has by about 50% higher electron density in the BCP (0.097 vs 0.063 in the Ru–Cl BCP).

D. Rate of hydration process

Activation barriers can give an estimation of the rate constants using Eyring's transition state theory [Eq. (4)].

TABLE III. Stabilization and binding energies of the ligands (in kcal/mol), a = NH_3, w = H_2O, ben = benzene, en and pta ligands are defined in the text. The calculations were done at the B3LYP/BS2/CPCM level.

	Stab	Stex	Repulsion	Deformation		
Ru_en_Cl+w	409.4	435.1	18.2	7.6		
TS_en	394.3	417.6	14.3	9.0		
Ru_en_w+Cl	403.3	426.7	15.0	8.4		
Ru_pta_Cl2+w	417.8	444.5	21.7	5.0		
TS_pta1a	397.4	422.9	19.2	6.3		
TS_pta1d1	387.1	414.9	17.4	6.1		
Int1	392.7	416.2	15.7	5.9		
TS_pta1d2	394.5	422.4	16.9	7.4		
Ru_pta_Cl_w+Cl	404.9	435.0	23.3	6.8		
Ru_pta_Cl_w+w	398.8	423.7	19.6	5.3		
TS_pta2a	378.3	403.4	18.4	6.6		
TS_pta2d1	369.6	408.8	11.1	6.4		
Int2	375.5	411.5	16.5	6.6		
TS_pta2d2	381.1	409.2	16.9	7.1		
Ru_pta_w2+Cl	385.7	414.6	21.4	7.5		
Ru_pta_Cl_OH+w	426.8	449.5	19.7	5.8		
TS_pta2d1+OH	418.3	433.4	18.3	6.5		
Int2_OH	414.7	428.3	13.1	6.9		
TS_pta2d2_OH	415.2	431.2	16.3	7.4		
Ru_pta_OH_w+Cl	422.1	445.8	22.9	7.8		
Pt_a2_Cl2+w	407.1	440.5	32.6	0.8		
TS_cis1	391.8	423.2	30.6	0.8		
Pt_a2_Cl_w+Cl	399.1	423.1	21.3	2.6		
Pt_a2_Cl_w+w	395.6	415.1	19.5	1.0		
TS_cis2	371.2	390.8	19.6	1.0		
Pt_a2_2w+Cl	385.7	398.9	13.3	2.7		
Pt_a2_Cl_OH+w	435.1	454.3	17.7	1.6		
TS_cis2_OH	413.5	443.0	28.3	1.2		
Pt_a2_OH_w+Cl	422.1	449.8	25.2	2.5		
	Cl		ben	en	w	
Ru_en_Cl+w	46.7		72.7	99.3	4.4	
TS_en	21.3		87.4	104.8	7.0	
Ru_en_w+Cl	19.2		81.5	110.0	34.1	
	Cl	Cl	ben	pta	w/h	w
Ru_pta_Cl2+w	42.0	42.0	59.1	42.0	5.2	
TS_pta1a	47.6	16.8	71.6	46.9	4.9	
TS_pta1d1	49.1	12.5	78.4	48.2	5.9	
Int1	51.2	5.6	92.7	53.6	5.6	
TS_pta1d2	48.1	5.8	90.9	50.1	4.6	
Ru_pta_Cl_w+Cl	46.6	16.7	65.7	45.8	31.4	
Ru_pta_Cl_w+w	51.7		67.1	45.8	30.0	10.4
TS_pta2a	22.7		81.8	47.9	21.0	13.5
TS_pta2d1	*39*		67.7	49.0	20.7	1.5
Int2	13.1		86.6	55.3	37.8	14.1
TS_pta2d2	8.4		93.8	52.4	26.4	12.4
Ru_pta_w2+Cl	20.1		76.2	51.4	24.0	38.8
Ru_pta_Cl_OH+w	12.0		73.6	52.9	24.1	17.1
TS_pta2d1+OH	26.6		57.1	37.8	67.5[a]	9.0
Int2_OH	5.6		77.7	43.2	83.1[a]	7.5
TS_pta2d2_OH	4.1		85.5	46.6	91.9[a]	7.5
Ru_pta_OH_w+Cl	5.1		86.6	41.7	85.8[a]	5.1
	Cl	Cl	NH3	NH3	w/h	w
Pt_a2_Cl2+w	48.7	48.7	54.8	54.8	7.7	
TS_cis1	15.0	53.8	54.1	51.1	3.4	
Pt_a2_Cl_w+Cl	19.7	57.8	59.4	66.8	42.9	

TABLE III. (Continued).

	Cl	Cl	NH3	NH3	w/h	w
Pt_a2_Cl_w+w		60.7	59.8	69.1	41.7	13.7
TS_cis2		27.7	62.3	72.6	37.0	7.8
Pt_a2_2w+Cl		28.8	73.2	73.2	45.9	45.9
Pt_a2_Cl_OH+w		50.6	54.8	51.8	89.4[a]	10.4
TS_cis2_OH		12.1	53.1	50.1	86.8[a]	10.1
Pt_a2_OH_w+Cl		18.2	54.4	62.6	84.5[a]	40.1

[a]Hydroxo ligand.

Based on this equation, rate constants for pseudo-first order hydration process were evaluated and collected in the gray lines of Table II. According to these constants the fastest hydration in the first reaction step occurs in the case of RAPTA complex; hydration of the Ru_en complex is about one order of magnitude slower. Hydration of cisplatin is, according to our calculations, the slowest process.

Rate constants can be easily compared with experimental values. Recently published rate constants for hydration of RAPTA-C (k_1=3.33 ± 0.02 × 10^{-3} and k_2=5.5 ± 0.2 × 10^{-2} s^{-1}) can give a good estimation of hydration of structurally similar complexes of RAPTA-B.[88] Slightly lower rate constant (k_{e1}=1.98 ± 0.02 × 10^{-2} s^{-1}) was obtained for hydration of Ru(arene)(en)Cl_2 complexes was obtained in Sadler's group.[19] As to cisplatin hydration, several measurements were performed,[89–93] estimating the k_{1c} constant between 5.2×10^{-5} and $1.9 \pm 0.2 \times 10^{-4}$ s^{-1}. Measurements of the second hydration step lead to the k_{2c}

TABLE IV. Critical points of all the M–L bonds (in *e*/a.u.^{3}). The analyses were done at the B3LYP/B2/CPCM level.

	Ru–N1[a]	Ru–N2	Ru–Cl	Ru–C[b]	Ru–O	
Ru_en_Cl+w	0.090	0.088	0.061	0.082		
TS_en	0.092	0.093	0.016	0.086	0.018	
Ru_en_w+Cl	0.091	0.092		0.082	0.068	
	Ru–P	Ru–Cl	Ru–Cl	Ru–C[d]	Ru–O	Ru–O
Ru_pta_Cl2+w	0.098	0.062	0.062	0.082		
TS_pta1a	0.097	0.067	0.014	0.090	0.017	
TS_pta1d1	0.096	0.075	0.007	0.089		
Int1	0.096	0.078		0.088		
TS_pta1d2	0.093	0.082		0.090		
Ru_pta_Cl_w+Cl	0.098	0.066		0.082	0.071	
Ru_pta_Cl_w+w	0.098	0.065		0.082	0.067	
TS_pta2a	0.096	0.017		0.089	0.064	0.023
TS_pta2d1	0.095	0.008		0.089	0.074	
Int2	0.093			0.089	0.086	
TS_pta2d2	0.091			0.089	0.072	
Ru_pta_w2+Cl	0.096			0.083	0.066	0.074
Ru_pta_Cl_OH+w	0.100	0.059		0.083	0.092	
TS_pta2d1+OH	0.093	0.010		0.089	0.119	
Int2_OH	0.093			0.089	0.132	
TS_pta2d2_OH	0.092			0.090	0.129	
Ru_pta_OH_w+Cl	0.097			0.082	0.099	0.068
	Pt–N[c]	Pt–N[d]	Pt–Cl	Pt–Cl	Pt–O	Pt–O[e]
Pt_a2_Cl2+w	0.117	0.117	0.086	0.085		
TS_cis1	0.124	0.118	0.086	0.038	0.043	
Pt_a2_Cl_w+Cl	0.126	0.116	0.088		0.093	
Pt_a2_Cl_w+w	0.113	0.125	0.087			0.088
TS_cis2	0.126	0.127	0.031		0.030	0.085
Pt_a2_2w+Cl	0.124	0.124			0.088	0.088
Pt_a2_Cl_OH+w	0.116	0.112	0.085			0.115
TS_cis2_OH	0.121	0.107	0.025		0.048	0.122
Pt_a2_OH_w+Cl	0.127	0.109			0.092	0.122

[a]*N* atom involved in H-bond interactions.
[b]Averaged value of BCPs.
[c]*N* atom in equatorial plane of TS or in H-bond interactions.
[d]*N* atom in axial position of TS.
[e]O from hydroxo ligand.

TABLE V. Natural population analysis of the key atoms (in *e*). The analyses were done at the B3LYP/B2/CPCM level.

	Ru	Cl		N1	N2	O	Benzene[a]
Ru_en_Cl+w	0.394	−0.590		−0.802	−0.790	−1.027	0.493
TS_en	0.553	−0.838		−0.812	−0.808	−1.030	0.577
Ru_en_w+Cl	0.493	−0.869		−0.803	−0.787	−0.942	0.531
	Ru	Cl	Cl	P	O	O	Benzene[a]
Ru_pta_Cl2+w	0.095	−0.568	−0.561	1.153		−1.046	0.483
TS_pta1a	0.260	−0.544	−0.831	1.101		−1.032	0.568
TS_pta1d1	0.242	−0.512	−0.907	1.035		−1.014	0.625
Int1	0.233	−0.494	−0.951	1.013		−1.012	0.646
TS_pta1d2	0.234	−0.481	−0.948	1.010		−0.994	0.634
Ru_pta_Cl_w+Cl	0.200	−0.548	−0.880	1.131		−0.929	0.513
Ru_pta_Cl_w+w	0.204		−0.546	1.122	−0.935	−1.010	0.536
TS_pta2a	0.354		−0.796	1.065	−0.924	−1.030	0.639
TS_pta2d1	0.372		−0.855	1.006	−0.990	−0.896	0.674
Int2	0.390		−0.918	0.968	−0.992	−0.889	0.713
TS_pta2d2	0.398		−0.942	0.967	−0.998	−0.882	0.746
Ru_pta_w2+Cl	0.311		−0.858	1.094	−0.940	−0.907	0.593
Ru_pta_Cl_OH+w	0.206		−0.601	1.173	−1.034	−1.002	0.392
TS_pta2d1+OH	0.377		−0.912	1.031	−1.029	−0.966	0.519
Int2_OH	0.352		−0.968	0.995	−1.030	−0.926	0.554
TS_pta2d2_OH	0.359		−0.957	1.015	−0.995	−0.935	0.533
Ru_pta_OH_w+Cl	0.294		−0.916	1.118	−0.892	−1.014	0.440
	Pt	Cl	Cl	N	N	O	O[b]
Pt_a2_Cl2+w	0.542	−0.615	−0.613	−1.027	−1.030	−1.035	
TS_cis1	0.710	−0.607	−0.839	−1.026	−1.007	−1.016	
Pt_a2_Cl_w+Cl	0.659	−0.602	−0.833	−1.049	−0.999	−0.961	
Pt_a2_Cl_w+w	0.669		−0.600	−0.946	−0.894	−0.976	−0.891
TS_cis2	0.812		−0.818	−0.897	−0.889	−0.975	−0.892
Pt_a2_2w+Cl	0.782		−0.801	−0.903	−0.903	−0.911	−0.911
Pt_a2_Cl_OH+w	0.645		−0.627	−1.039	−1.034	−1.072	−1.106
TS_cis2_OH	0.795		−0.881	−1.056	−1.004	−1.000	−1.105
Pt_a2_OH_w+Cl	0.735		−0.848	−1.062	−0.999	−0.964	−1.113

[a]Sum of partial charges of all C and H atoms.
[b]O of hydroxo group.

value of $1.1 \pm 0.1 \times 10^{-4}$.[89,92,94] It is probably not necessary to mention that the differences can be made by various experimental settings. While computational estimations of the rate constants for the first reaction steps are in acceptable agreement with measured data, calculated values for the second steps are substantially worse for cisplatin. In the RAPTA case, fairly good agreement was obtained for dissociation mechanism in neutral and acidic condition where aqua ligand is present. However, a different complex is considered as a reactant under the experimental conditions where authors[88] expect a hydration of the neutral complex with the negatively charged hydroxo group instead of the aqua ligand. Calculations with the neutral RAPTA complex lead to very fast reaction cause with rate constant $k_2 \approx 3 \times 10^3$ s^{-1}. The explanation can be searched in stronger Ru–OH coordination which represents a higher competition to the Ru–Cl interaction and facilitates a release of chloride particle and its replacement by second aqua ligand.

E. Properties of electron density

To complete the comparison of the hydration reactions of the chosen metal complexes several analyses were performed for all the stationary points on the reaction coordinates. Electron densities of the most important BCPs are collected in Table IV and charges obtained in the framework of natural population analysis are summarized in Table V.

Correlation between BEs and BCPs was already discussed above. Nevertheless, it is worth to note that in the RAPTA complexes, only three BCPs of the Ru–C bonds were found (with exception of the reaction product of the second step where already two relatively weaker aqua ligands are coordinated so that a stronger benzene coordination can occur). On the other hand in all the Ru_en complexes four BCPs were found.

It can be also mentioned that in accord with higher coordination, lower BCP densities for metal coordination of replacing ligands were obtained in TSs of Ru(II) complexes (both Ru–O and Ru–Cl bonds have ≈0.02 *e*/a.u.^{3}) in comparison with Pt(II) complexes (where values of 0.04 were acquired). Basically all BCP densities are visibly higher in cisplatin complexes in comparison with Ru(II) complexes due to lower ligand competition. The same conclusion can be also drawn from the BE decomposition.

Results of the NPA analysis for individual metal complexes are summarized in Table V. From partial charges of

metal cations it follows that while the charge of the Pt atom varies between 0.55 and 0.8 *e* in dependence on donation strength of coordinated ligands, the Ru charges of the Ru_en complexes lie in the range of 0.4–0.55 *e*. The lowest metal charges were found in the RAPTA complexes with values from 0.1 to 0.35 *e*. (In analogous analysis at the MP2/6-31++G(d,p) computational level even negative values were obtained for most of the RAPTA complexes.)

From Table V an estimation of electrostatic strengthening of the coordination-covalent bonds can be judged based on the Coulomb law. Since the covalent character of the bond basically follows from a BCP value, at least, an approximate estimation of the prevailing contributions to the given coordination can be ensued from Tables IV and V.

III. CONCLUSIONS

In this study hydration reactions and electronic properties of three different organometallic complexes were subject to quantum chemical calculations.

All the complexes were optimized at the B3LYP/6-31G(d)/CPCM level where metal atoms were treated with Stuttgart effective core potentials (ECPs). The SP energy calculations and determination of electronic properties were performed at the B3LYP/6-311++G(2df,2pd)/CPCM level.

It was found that our hydration model works fairly well for the replacement of the first chloride by water molecule—acceptable agreement for both Gibbs free energies and rate constants was obtained. In the second hydration step a visibly underestimated value of cisplatin rate constant can be noticed. On the contrary in direct dissociation mechanism in basic environment too fast dechlorination is predicted due to more strongly coordinated hydroxo ligand.

For the comparison of the hydration reaction of all three complexes, stabilization and binding energies together with BCP electron densities and NPA partial charges were evaluated in all stationary points of the reaction coordinates. Estimated BEs confirm that the benzene ligand is relatively weakly bonded assuming the fact that arene ligand occupies three and four coordination positions of the Ru(II) cation in the RAPTA and Ru_en complexes, respectively. In this way, this coordination has similar strength like coordination of the aqua ligand. The strongest coordination of the chloride ligand occurs in cisplatin complex in accord with the lowest rate constants (the highest activation barrier). The BE of the Ru–Cl bond in the Ru_en complex is by about 2 kcal/mol lower, which correlates well with faster hydration course in this complex and the fastest activation reaction in the RAPTA case is connected with the most "loosely" interacting chloride. From the point of BEs of chloride ligands, the higher barriers in the second reaction step are not surprising.

Basically all the relations in binding energies correlate with NPA partial charges and AIM analysis of BCPs as follows from the discussion above.

ACKNOWLEDGMENTS

Authors are grateful for support provided by the MŠMT Project MSM 0021620835 and by GA ČR Project P205/10/0228 (JVB, ZF) and MŠMT Project Nos. ME10149 (JVB) and ME09062(ZCh).

Calculations were partly performed at the Metacentrum. The access to this supercomputer center provided under the research intent MSM6383917201 is highly appreciated.

[1] J. Reedijk and J. M. Teuben, in *Cisplatin*, edited by B. Lippert (Wiley-VCH, Weinheim, 1999).
[2] A. W. Prestayko, J. C. D'Aoust, B. F. Issell, and S. T. Crooke, Cancer Treat. Rev. **6**, 17 (1979).
[3] J. R. Rubin, T. P. Haromy, and M. Sundaralingam, Acta Crystallogr. Sect. C: Cryst. Struct. Commun. **47**, 1712 (1991).
[4] J. M. Asara, J. S. Hess, E. Lozada, K. R. Dunbar, and J. Allison, J. Am. Chem. Soc. **122**, 8 (2000).
[5] D. M. L. Goodgame, C. A. Omahoney, C. J. Page, and D. J. Williams, Inorg. Chim. Acta **175**, 141 (1990).
[6] N. Katsaros and A. Anagnostopoulou, Crit. Rev. Oncol. Hematol. **42**, 297 (2002).
[7] K. Sorasaenee, J. R. Galan-Mascaros, and K. R. Dunbar, Inorg. Chem. **41**, 433 (2002).
[8] M. Uudsemaa and T. Tamm, Chem. Phys. Lett. **342**, 667 (2001).
[9] F. Caruso and M. Rossi, Mini Rev. Med. Chem. **4**, 49 (2004).
[10] B. M. zu Berstenhorst, G. Erker, G. Kehr, J. C. Wasilke, J. Muller, H. Redlich, and J. Pyplo-Schnieders, Eur. J. Inorg. Chem. **1**, 92 (2005) .
[11] M. Hartmann, A. Robert, V. Duarte, B. K. Keppler, and B. Meunier, J. Biol. Inorg. Chem. **2**, 427 (1997).
[12] P. Lincoln and B. Norden, J. Phys. Chem. B **102**, 9583 (1998).
[13] K. Gisselfaelt, P. Lincoln, B. Norden, and M. Jonsson, J. Phys. Chem. B **104**, 3651 (2000).
[14] J.-G. Liu, B.-H. Ye, Q.-L. Zhang, X.-H. Zou, Q.-X. Zhen, X. Tian, and L.-N. Ji, J. Biol. Inorg. Chem. **5**, 119 (2000).
[15] J. Malina, O. Novakova, B. K. Keppler, E. Alessio, and V. Brabec, J. Biol. Inorg. Chem. **6**, 435 (2001).
[16] A. Kueng, T. Pieper, R. Wissiack, E. Rosenberg, and B. K. Keppler, J. Biol. Inorg. Chem. **6**, 292 (2001).
[17] H. M. Chen, J. A. Parkinson, R. E. Moris, and P. J. Sadler, J. Am. Chem. Soc. **125**, 173 (2003).
[18] O. Novakova, H. Chen, O. Vrana, A. Rodger, P. J. Sadler, and V. Brabec, Biochemistry **42**, 11544 (2003).
[19] F. Wang, H. M. Chen, S. Parsons, L. D. H. Oswald, J. E. Davidson, and P. J. Sadler, Chem. Eur. J. **9**, 5810 (2003).
[20] V. G. Vaidyanathan and B. U. Nair, J. Inorg. Biochem. **91**, 405 (2002).
[21] B. Serli, E. Zangrando, T. Gianferrara, C. Scolaro, P. J. Dyson, A. Bergamo, and E. Alessio, Eur. J. Inorg. Chem. **17**, 3423 (2005).
[22] T. Bugarcic, A. Habtemariam, J. Stepankova, P. Heringova, J. Kasparkova, R. J. Deeth, R. D. L. Johnstone, A. Prescimone, A. Parkin, S. Parsons, V. Brabec, and P. J. Sadler, Inorg. Chem. **47**, 11470 (2008).
[23] S. S. N. Kraft, C. Bischof, A. Loos, S. Braun, N. Jafarova, and U. Schatzschneider, J. Inorg. Biochem. **103**, 1126 (2009).
[24] A. K. Renfrew, A. D. Phillips, E. Tapavicza, R. Scopelliti, U. Rothlisberger, and P. J. Dyson, Organometallics **28**, 5061 (2009).
[25] A. F. A. Peacock, A. Habtemariam, R. Fernandez, V. Walland, F. P. A. Fabbiani, S. Parsons, R. E. Aird, D. I. Jodrell, and P. J. Sadler, J. Am. Chem. Soc. **128**, 1739 (2006).
[26] A. Dorcier, P. J. Dyson, C. Gossens, U. Rothlisberger, R. Scopelliti, and I. Tavernelli, Organometallics **24**, 2114 (2005).
[27] R. Wysokinski and D. Michalska, J. Comput. Chem. **22**, 901 (2001).
[28] P. N. Pavankumar, P. Seetharamulu, S. Yao, J. D. Saxe, D. G. Reddy, and F. H. Hausheer, J. Comput. Chem. **20**, 365 (1999).
[29] H. F. Dos Santos, B. L. Marcial, C. F. De Miranda, L. A. S. Costa, and W. B. De Almeida, J. Inorg. Biochem. **100**, 1594 (2006).
[30] L. A. S. Costa, W. R. Rocha, W. B. De Almeida, and H. F. Dos Santos, J. Inorg. Biochem. **99**, 575 (2005).
[31] Z. Chval, M. Sip, and J. V. Burda, J. Comput. Chem. **29**, 2370 (2008).
[32] M. Zeizinger, J. V. Burda, J. Šponer, V. Kapsa, and J. Leszczynski, J. Phys. Chem. A **105**, 8086 (2001).
[33] J. Raber, C. Zhu, and L. A. Eriksson, J. Phys. Chem. **109**, 11006 (2005).
[34] A. Robertazzi and J. A. Platts, J. Comput. Chem. **25**, 1060 (2004).
[35] Y. Zhang, Z. Guo, and X.-Z. You, J. Am. Chem. Soc. **123**, 9378 (2001).
[36] J. V. Burda, M. Zeizinger, and J. Leszczynski, J. Comput. Chem. **29**, 907 (2005).

[37]J. V. Burda, M. Zeizinger, and J. Leszczynski, J. Chem. Phys. **120**, 1253 (2004).
[38]G. Schroeder, J. Kozelka, M. Sabat, M.-H. Fouchet, R. Beyerle-Pfnur, and B. Lippert, Inorg. Chem. **35**, 1647 (1996).
[39]J. F. Lopes, V. S. D. Menezes, H. A. Duarte, W. R. Rocha, W. B. De Almeida, and H. F. Dos Santos, J. Phys. Chem. B **110**, 12047 (2006).
[40]J. V. Burda and J. Leszczynski, Inorg. Chem. **42**, 7162 (2003).
[41]M. Zeizinger, J. V. Burda, and J. Leszczynski, Phys. Chem. Chem. Phys. **6**, 3585 (2004).
[42]M.-H. Baik, R. A. Friesner, and S. J. Lippard, J. Am. Chem. Soc. **124**, 4495 (2002).
[43]M. H. Baik, R. A. Friesner, and S. J. Lippard, Inorg. Chem. **42**, 8615 (2003).
[44]M. H. Baik, R. A. Friesner, and S. J. Lippard, J. Am. Chem. Soc. **125**, 14082 (2003).
[45]M. Eriksson, M. Leijon, C. Hiort, B. Norden, and A. Graeslund, Biochemistry **33**, 5031 (1994).
[46]M. Coll, S. E. Sherman, D. Gibson, S. J. Lippard, and A. H.-J. Wang, J. Biomol. Struct. Dyn. **8**, 315 (1990).
[47]K. Spiegel, U. Rothlisberger, and P. Carloni, J. Phys. Chem. B **108**, 2699 (2004).
[48]A. Robertazzi and J. A. Platts, Inorg. Chem. **44**, 267 (2005).
[49]Z. Chval and M. Šíp, J. Mol. Struct.: THEOCHEM **532**, 59 (2000).
[50]Z. Chval and M. Šíp, Collect. Czech. Chem. Commun. **68**, 1105 (2003).
[51]M. Pavelka, M. Šimánek, J. Šponer, and J. V. Burda, J. Phys. Chem. A **110**, 4795 (2006).
[52]D. V. Deubel, J. Am. Chem. Soc. **126**, 5999 (2004).
[53]T. Zimmermann, M. Zeizinger, and J. V. Burda, J. Inorg. Biochem. **99**, 2184 (2005).
[54]T. Zimmermann and J. V. Burda, J. Chem. Phys. **131**, 135101 (2009).
[55]T. Zimmermann, Z. Chval, and J. V. Burda, J. Phys. Chem. B **113**, 3139 (2009).
[56]T. Zimmermann and J. V. Burda, Dalton Trans. **39**(5), 1295 (2010).
[57]C. Gossens, I. Tavernelli, and U. Rothlisberger, Chimia **59**, 81 (2005).
[58]D. V. Deubel and J. K. C. Lau, Chem. Commun. (23), 2451 (2006).
[59]J. C. Chen, L. M. Chen, S. Y. Liao, K. Zheng, and L. N. Ji, Dalton Trans. (32), 3507. (2007).
[60]J. C. Chen, L. M. Chen, S. Y. Liao, K. C. Zheng, and L. N. Ji, J. Mol. Struct.: THEOCHEM **901**, 137 (2009).
[61]J. C. Chen, L. M. Chen, S. Y. Liao, K. C. Zheng, and L. N. Ji, Phys. Chem. Chem. Phys. **11**, 3401 (2009).
[62]J. C. Chen, L. M. Chen, L. C. Xu, K. C. Zheng, and L. N. Ji, J. Phys. Chem. B **112**, 9966 (2008).
[63]C. Gossens, A. Dorcier, P. J. Dyson, and U. Rothlisberger, Organometallics **26**, 3969 (2007).
[64]C. Gossens, I. Tavernelli, and U. Rothlisberger, J. Phys. Chem. A **113**, 11888 (2009).
[65]R. Aird, J. Cummings, A. Ritchie, M. Muir, R. Morris, H. Chen, P. Sadler, and D. Jodrell, Br. J. Cancer **86**, 1652 (2002).
[66]S. J. Berners-Price, L. Ronconi, and P. J. Sadler, Prog. Nucl. Magn. Reson. Spectrosc. **49**, 65 (2006).
[67]H. Chen, J. A. Parkinson, S. Parsons, R. A. Coxal, R. O. Gould, and P. Sadler, J. Am. Chem. Soc. **124**, 3064 (2002).
[68]J. Kašparková, F. S. Mackay, V. Brabec, and P. J. Sadler, J. Biol. Inorg. Chem. **8**, 741 (2003).
[69]A. Habtemariam, M. Melchart, R. Fernandez, S. Parsons, I. D. H. Oswald, A. Parkin, F. P. A. Fabbiani, J. E. Davidson, A. Dawson, R. E. Aird, D. I. Jodrell, and P. J. Sadler, J. Med. Chem. **49**, 6858 (2006).
[70]F. Y. Wang, A. Habtemariam, E. P. L. Van Der Geer, R. Fernandez, M. Melchart, R. J. Deeth, R. Aird, S. Guichard, F. P. A. Fabbiani, P. Lozano-Casal, I. D. H. Oswald, D. I. Jodrell, S. Parsons, and P. J. Sadler, Proc. Natl. Acad. Sci. U.S.A. **102**, 18269 (2005).
[71]A. B. Chaplin, C. Fellay, G. Laurenczy, and P. J. Dyson, Organometallics **26**, 586 (2007).
[72]C. A. Vock and P. J. Dyson, Z. Anorg. Allg. Chem. **633**, 640 (2007).
[73]K. Gkionis, J. A. Platts, and J. G. Hill, Inorg. Chem. **47**, 3893 (2008).
[74]R. E. Morris, R. E. Aird, P. D. Murdoch, H. M. Chen, J. Cummings, N. D. Hughes, S. Parsons, A. Parkin, G. Boyd, D. I. Jodrell, and P. J. Sadler, J. Med. Chem. **44**, 3616 (2001).
[75]Z. Futera, J. Klenko, J. E. Šponer, J. Šponer, and J. V. Burda, J. Comput. Chem. **30**, 1758 (2009).
[76]R. F. W. Bader, *Atoms in Molecules: A Quantum Theory* (Oxford University, Oxford, 1990).
[77]C. S. Allardyce, P. J. Dyson, D. J. Ellis, and S. L. Heath, Chem. Commun. 1396 (2001).
[78]C. S. Allardyce, P. J. Dyson, D. J. Ellis, P. A. Salter, and R. Scopelliti, J. Organomet. Chem. **668**, 35 (2003).
[79]A. Klamt, J. Phys. Chem. **99**, 2224 (1995).
[80]A. Klamt and G. Schuurmann, J. Chem. Soc., Perkin Trans. **2** (5), 799 (1993).
[81]D. Andrae, U. Haussermann, M. Dolg, H. Stoll, and H. Preuss, Theor. Chim. Acta **77**, 123 (1990).
[82]A. Bergner, M. Dolg, W. Kuechle, H. Stoll, and H. Preuss, Mol. Phys. **80**, 1431 (1993).
[83]J. V. Burda, M. Zeizinger, J. Šponer, and J. Leszczynski, J. Chem. Phys. **113**, 2224 (2000).
[84]T. A. Keith AIMAll (Version 10.11.24) 2010 (aim.tkgristmill.com).
[85]E. D. Glendening, J. K. Badenhoop, A. E. Reed, J. E. Carpenter, J. A. Bohmann, C. M. Morales, and F. Weinhold, *NBO 5.0* University of Wisconsin, Madison (2001).
[86]B. Cordero, V. Gómez, A. E. Platero-Prats, M. Revés, J. Echeverría, E. Cremades, F. Barragán, and S. Alvarez, Dalton Trans. **21**, 2832 (2008).
[87]A. E. Egger, C. G. Hartinger, A. K. Renfrew, and P. J. Dyson, J. Biol. Inorg. Chem. **15**, 919 (2010).
[88]C. Scolaro, C. G. Hartinger, C. S. Allardyce, B. K. Keppler, and P. J. Dyson, J. Inorg. Biochem. **102**, 1743 (2008).
[89]J. Arpalahti, M. Mikola, and S. Mauristo, Inorg. Chem. **32**, 3327 (1993).
[90]K. Hindmarsh, D. A. House, and M. M. Turnbull, Inorg. Chim. Acta **257**, 11 (1997).
[91]J.-L. Jestin, B. Lambert, and J.-C. Chottard, J. Biol. Inorg. Chem. **3**, 515 (1998).
[92]E. Segal-Bendirdjian, P. Brehin, B. Lambert, A. Laousi, J. Kozelka, M. Barreau, F. Lavalle, J. B. LePecq, and J.-C. Chottard, *Platinum and Other Metal Coordination Compounds in Cancer Chemotherapy* (Plenum, New York, 1991).
[93]D. P. Bancroft, C. A. Lepre, and S. J. Lippard, J. Am. Chem. Soc. **112**, 6860 (1990).
[94]N. P. Johnson, J. D. Hoeschele, and R. O. Rahn, Chem. Biol. Interact. **30**, 151 (1980).

Binding of Piano–Stool Ru(II) Complexes to DNA; QM/MM Study

Zdeněk Futera[1], James A. Platts[2], Jaroslav V. Burda[1*]

[1]Department of Chemical Physics and Optics, Faculty of Mathematics and Physics, Charles University, Ke Karlovu 3, 121 16 Prague 2, Czech Republic

[2]School of Chemistry, Cardiff University, Park Place, Cardiff CF10 3AT, U.K.

Abstract

Ru(II) "piano–stool" complexes belong to group of biologically active metallocomplexes with promising anticancer activity. In this study, we investigate the reaction mechanism of $[(\eta^6\text{-benzene})Ru^{II}(en)(H_2O)]^{2+}$ (en = ethylenediamine) complex binding to DNA by hybrid QM/MM computational techniques. The reaction when the Ru(II) complex is coordinated on N7–guanine from major groove is explored. Two reaction pathways, direct binding to N7 position and two–step mechanism passing through O6 position, are considered. It was found that the reaction is exothermic and the direct binding process is preferred kinetically. In analogy to cisplatin, we also explored the possibility of intrastrand cross–link formation where the Ru(II) complex makes a bridge between two adjacent guanines. Two different pathways were found, leading to a final structure with released benzene ligand. This process is exothermic; however, one pathway is blocked by relatively high initial activation barrier. Geometries, energies and electronic properties analyzed by atoms in molecules and natural population analysis methods are discussed.

Keywords: Ruthenium(II) complexes, piano–stool structure, intrastrand cross–link, hybrid QM/MM computational method, ONIOM, DFT

Introduction

Transition metal complexes are widely used as drugs in pharmacology because of their high coordination numbers and strong interactions with bioorganic materials [1, 2]. This is especially the case in cancer treatment, where cisplatin (*cis*-diamminedichloroplatinum(II), Fig. 1) was approved as a chemotherapeutic drug in 1970s [3, 4]. Despite the great success of this drug, its behaviour in living organisms is far from satisfactory due to many negative side effects, such as nephrotoxicity, neurotoxicity, ototoxicity, and myelosuppression. Moreover, cisplatin is efficient only against some types of tumours including testicular and ovarian cancer, bladder tumours, melanoma, non-small cell lung cancer, small cell lung cancer, lymphomas and myelomas [5]. Many other kinds of cancer are resistant to treatment by cisplatin, for example, colorectal or pancreatic carcinoma [6].

*Corresponding author. Tel.: +42021911246; Fax: +420221911249; Email: burda@karlov.mff.cuni.cz

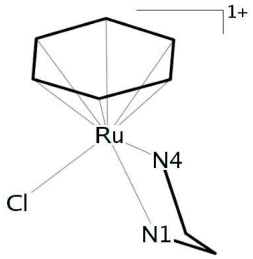

Table 1: $[(\eta^6\text{-benzene})\text{Ru}^{\text{II}}(\text{en})\text{Cl}]^+$ (en = ethylenediamine) complex, for its shape usually called Ru(II) "piano–stool" complex.

Therefore, research of complexes with better properties and fewer side-effects is very intensive. Many new platinum based drugs have been invented, and some of them are extensively used in medical practice (such as carboplatin and oxaliplatin [5, 7, 8]). Reaction mechanisms of cisplatin in a cell have been studied both experimentally [9–12] and theoretically [13–24] and its activity explained more or less satisfactorily.

When cisplatin enters the cell, passing through cellular membrane, first the hydration reaction occurs (see Fig. 1a). This is termed activation because the hydrated platinum complex is much more reactive than cisplatin itself and can interact with numerous compounds in the cell (such as RNA, DNA, proteins or peptides [25]). However, penetration into a nucleus and binding to DNA is most important for anti-cancer activity. It was shown that the preferred coordination site is nitrogen N7 of guanine, which can be easily approached in major groove. If there are neighbouring guanines, cisplatin may create the so called intrastrand cross–link structure which is a bridge between N7 nitrogens of two adjacent guanines [26–29], as shown in Fig. 1b. This bridge is crucial for cytostatic activity, because it causes local deformation of DNA, blocking a transcription part of replication process and can finally lead to apoptosis of the cell.

A group of ruthenium complexes with the so called "piano–stool" structure (see Fig. 1) was discovered at the beginning of the last decade [30, 31], and their cytotoxicity was experimentally proven [32, 33]. The behaviour of these compounds is to some extent similar to cisplatin. The Ru(II) complex also undergoes the hydration reaction in the cell environment, in which the chlorine is replaced by water, and subsequently interacts with DNA. Similarly to cisplatin, the N7 position of guanine is the most preferable for binding [34, 35]. Although the chelate (en) ring stabilizes the structure of the Ru(II) complex [36], the arene ligand can participate in interaction with DNA [37, 38] and influence the anti-cancer activity [39]. However, in contrary to all these known facts the whole cytostatic mechanism of these complexes is still not completely known.

In this computational study we focus on the already hydrated $[(\eta^6\text{-benzene})\text{Ru}^{\text{II}}\text{-}(\text{en})(\text{H}_2\text{O})]^{2+}$ complex and its interaction with DNA using QM/MM computational approach. Our work has two parts. First, the fundamental reaction is explored when the Ru(II) complex is bound to N7 nitrogen of guanine. Two possible pathways of this process leading to the Ru(II)–N7(G) mono–adduct were suggested in previous works [35, 40]. It is a diret binding crossing single energy barrier or more complicated two–step mecdhanism where first Ru(II)–O6(G) intermediate structure is formed and then transition to N7 position proceeds. Both these pathways are shown in Fig. 2 and are considered in calculations presented here.

The second part of this article is devoted to an investigation of Ru(II) complexes when the intrastrand CL between two adjacent guanines is formed, in anal-

ogy to cisplatin. Because Ru(II) piano–stool complexes are monofunctional, Ru(II)–N7(G) mono–adduct cannot be transformed into CL without at least partial release of Ru(II) coordination to arene. Ethylenediamine is important for guanine base recognition and its interaction with Ru(II) cation is relatively strong in comparison to benzene ligand. Therefore, we suggest a reaction mechanism, where the benzene is releasing. First, η^6–coordination of the benzene, formally occupying three coordination sites, is transformed into η^2 type. Two vacant sites are available after this structure rearrangement. One of them is used to N7 coordination of the second guanine (G2) while the second one can be saturated by interation with O6(G2) oxygen or with water molecule as shown in Fig. 3. Finally, the guanine–guanine CL structure where the benzene ligand is fully released and water molecule binds the remaining vacant valence.

Computational Details

Piano–stool Ru(II) complexes, their hydration and consequent interaction with DNA were already studied by our group at QM level [35]. In that work, a relatively small computational model was used, concentrating only on the Ru(II) complex with guanine at the B3LYP/6-31++G(d,p) level of calculations. This approach was sufficiently accurate for interaction energies and energy barriers (detailed comparison with experimental data is discussed in the study [35]), but the model lacked the steric and electrostatic interactions caused by molecular environment of DNA. As a result transition state for direct binding to N7 position of guanine was not found.

In this study, the hybrid QM/MM approach is used, which allows extension of the computational model by adding a larger fragment of DNA. A six base–pairs *ds*-DNA oligonucleotide was created using Amber NucGen tool [41] with standard B-DNA geometry parameters. A sequence with two adjacent guanine in the middle has been chosen: 5'-GCG*G*GC-3', the second strand is complementary according to Watson–Crick base pairing. Ten sodium cations were added to saturate negative charge of the sugar–phosphate backbone and the whole structure was relaxed by 100 ps MD run in water box using Amber FF96 [42, 43] and TIP3P model [44]. Temperature 298.15 K was kept by Langevin thermostat [45] during the sim-

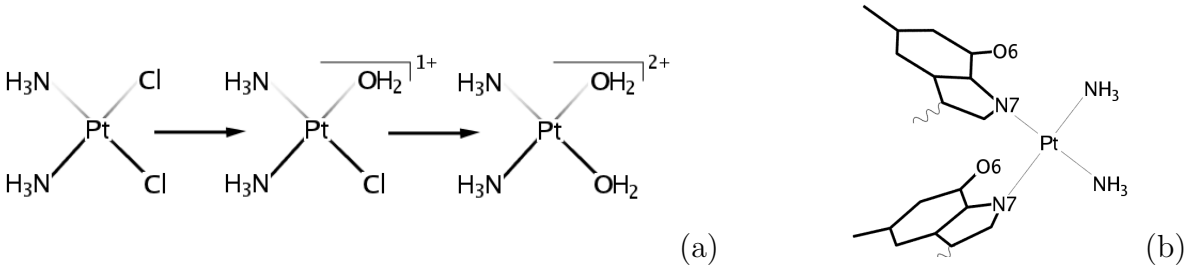

Figure 1: Cisplatin (*cis*–diamminedichloroplatinum(II) complex): (a) hydration to first and second grade which proceeds in cellular nucleus because of low Cl^- concentration, (b) intrastrand CL structure where cisplatin is bridging N7 nitrogens of two adjacent guanines.

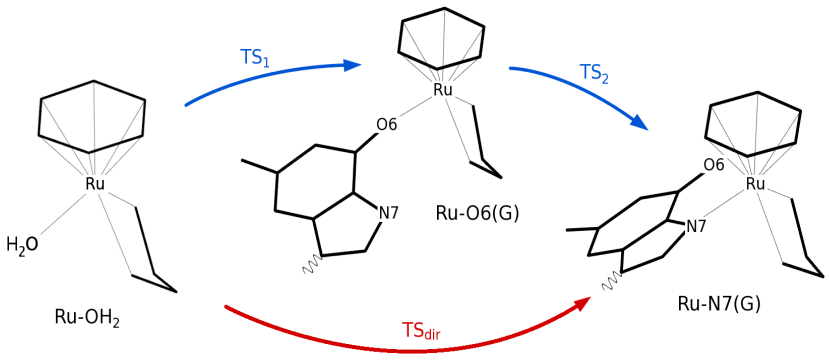

Figure 2: Reaction scheme of DNA ruthenization: activated Ru(II) piano–stool complex (Ru-OH_2) creates Ru-N7(G) adduct directly (red path) or undergoes two–step reaction mechanism through Ru-O6(G) (blue path).

ulation. After that, the whole system was minimized by conjugate gradient algorithm available in Amber package [41].

Equilibrated and minimized DNA structure was extracted from water box and the $[(\eta^6\text{-benzene})Ru^{II}(en)(H_2O)]^{2+}$ complex was docked to it manually, guided by structure parameters from previous study [35]. As the Ru(II) complex has charge 2+ only eight Na^+ cations were added to keep the whole system electroneutral. The resulting system was partitioned into QM part, including Ru(II) complex with two guanines, and MM part conatining the rest of the system (cf. Fig. 4). The ONIOM version of QM/MM technique [46, 47] implemented in Gaussian 09 [48] was used here. The QM model was evaluated at the BLYP/6-31G(d) DFT level using SDD basis set and ECP for the description of the Ru atom [49, 50], while the MM part is parametrized by Amber FF96 [43]. Unsaturated valence on N9 nitrogen of guanine, created when the glycosidic bond was broken on the QM–MM boundary, was capped by hydrogen link atoms. Electronic embedding is used in all ONIOM calculations.

Optimization of ONIOM model was done subsequently one structure after another as in reaction schemes in Fig. 2 and Fig. 3 to avoid geometry movements at the ends of DNA double–helix that would complicate energy comparison of these structures. That means that DNA with unbound Ru(II)–OH_2 complex in the vicinity of central guanine pair was fully optimized, then QM part of the model was rearranged to Ru(II)–O6(G) geometry and reoptimized with fixed MM part. Finally, the whole model was optimized without any constrain or restrain and the procedure continued by other structure.

After optimization of every stationary point in ONIOM model, the QM part was separated and reoptimized at B3LYP/6-31G(d) with implicit IEFPCM/UFF model of water solution. To keep the same arrangement of guanines as in ONIOM optimized structures with *ds*-DNA oligomer, the C2, O6 and N9 atoms of each guanine were fixed during the DFT reoptimization. Electron densities of final structures were analyzed at the B3LYP/6-31++G(d,f) level where also the SDD basis set on the Ru atom was extended by a set of diffuse functions with ex-

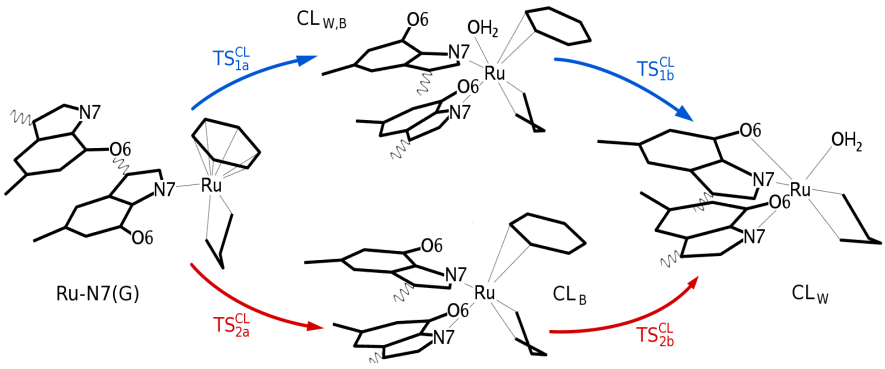

Figure 3: Reaction scheme Ru(II) cross–link formation where two reaction pathways leading to final CL_W are assumed: water molecule interacts with Ru(II) complex already in intermediate state $CL_{W,B}$ (blue path) or benzene ligand first change coordination from η^6 to η^2–type (CL_B) and then is substitued by water (red path).

ponents $\alpha(s) = 0.008$, $\alpha(p) = 0.011$ and $\alpha(d) = 0.025$.

Interaction energies of all ligands coordinated to central metal cation were calculated according to equation:

$$\Delta E^{BE}(L) = E_{complex} - E_L - E_{rest} \qquad (1)$$

where $E_{complex}$ is total energy of the whole QM complex and E_L and E_{rest} are BSSE corrected energies of isolated ligand and its complement. Deformation corrections are not considered. We are aware of the fact that such approach leads to some (systematic) overestimation of BE values. Conversely, relaxation of the metal complex without one ligand would end in some "imaginary" species with substantially modified electronic configuration of the central cation, which is completely irrelevant to original complex. Atoms in Molecules (AIM) [51–53] topological analysis of the critical point of electron density was performed by AIMAll program [54] and atomic partial charges were determined using Natural Population Analysis (NPA) [55, 56] method implemented in Gaussian 09. The combined charge and energy decomposition analysis [57] (ETS NOCV – Extended Transition State [58] with Natural Orbitals for Chemical Valence [59, 60]) as it is implemented in ADF program [61] was used for insight into binding picture of Ru complex with various ligands. BP88 functional [62] was combined with TZP basis set. Ru cation was described using Ru.3d core of scalar relativistic pseudopotentials based on ZORA approach.

Results and Discussion

Binding to DNA – Ru(II) adduct formation

First, the interaction of the activated Ru(II) aqua–complex with DNA is explored (see reaction scheme in Fig. 2). Binding to N7 nitrogen of guanine in major groove is assumed. We consider a direct reaction path with one transition state as well as a two–step reaction mechanism as suggested previously [35]. All stationary points on the reaction coordinate are optimized in ONIOM

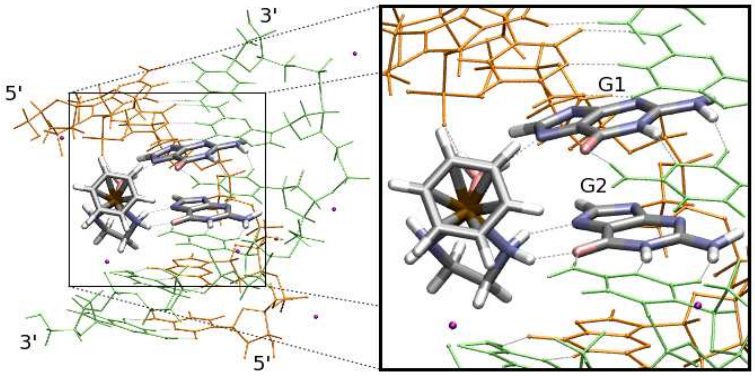

Figure 4: QM/MM partitioning of a computational model: QM part consisting of Ru(II) complex and two adjacent guanines is highlighted, MM part includes DNA double-helix (5'-GCG*G*GC-3' strand is drawn in orange color) and 8 Na^+ cations.

model and separated QM parts of the system reoptimized in PCM implicit solvent with fixed position of guanines as described above.

Structures

Important interatomic distances in optimized structures are collected in Tab. 2 and stable minima are shown in Fig. 5. The Ru(II) complex interacts with first guanine (G1, located toward the 5'–end base, see Fig. 4), as seen from Ru-N7 and Ru-O6 distances, while the second guanine (G2, closer to the 3'–end) is included in the model in order to take into account important steric and electrostatic effects and for comparison with CL structures discussed in next section.

In the reactant structure, the Ru(II) complex does not interact with DNA covalently but there are three hydrogen bonds. Both hydrogens from aqua ligand interact with O6 oxygen on G1 or G2 and one more H-bond is formed between N7(G1) and hydrogen on N4(en) (see Fig. 5a). This last H-bond makes the Ru-N1,N4(en) interaction asymmetric, as can seen from interatomic distances in Tab. 2. As part of the electron density from H-N4(en) is used for H-bonding, the Ru-N4(en) interaction is stronger, which results in shorter Ru-N4(en) distance than Ru-N1(en). Similar behaviour also appears in other structures.

In the intermediate structure as well as in product of the reaction, the aqua ligand is fully released from the complex. Longer distance of Ru-O(wat) in the case of ONIOM model, in comparison with reoptimized quantum–core structures, is caused by interaction of the released water with negatively charged phosphate group. The intermediate structure is stabilized by two H-bonds between hydrogens of (en) ligand and N7(G1) and O6(G2) while in the product structure there is only one H-bond to O6(G1). Such differences in distances between ONIOM and QM model are caused by "environmental" effects presented only in ONIOM model.

In the transition state of direct binding mechanism (TS_{dir}), the position of ethylenediamine is stabilized by two hydrogen bonds to N7(G2) and O6(G2). Hydrogens from the aqua ligand interact with oxygens O6

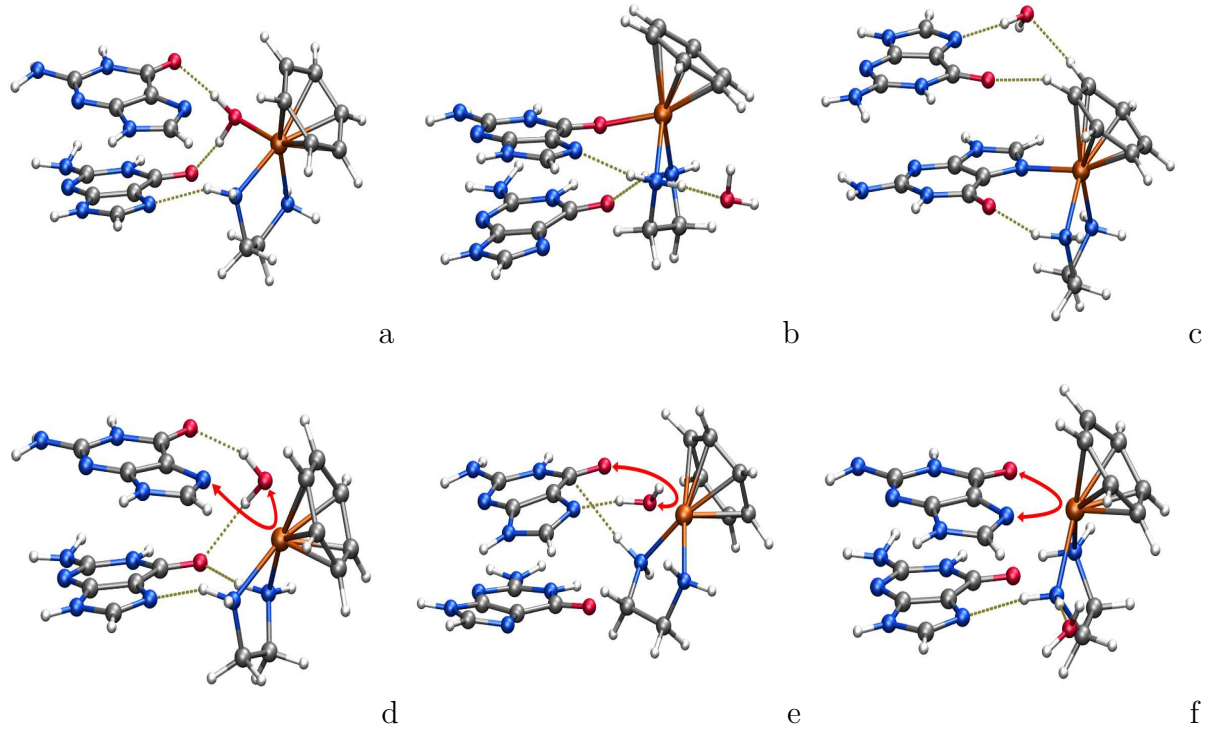

Figure 5: Optimized stationary points of reaction where the Ru complex binds to DNA (see reaction scheme in Fig. 2), both central guanines are shown: (a)free Ru-OH_2 , (b) Ru-O6(G) adduct, (c) Ru-N7(G) adduct, (d) TS_{dir}, (e) TS_1, (f) TS_2.

of both guanines. Thus, the Ru complex uses all guanine H-bond acceptor sites in major groove for structure stabilization. The distance of the central metal cation from N7(G1) is already shorter than Ru-O(wat).

In the two–step reaction mechanism there are two transition states ($TS_{1,2}$, see reaction scheme in Fig. 2). First the Ru(II) complex interacts with O6 passing through TS_1. On the contrary to situation in TS_{dir}, the Ru cation is closer to aqua ligand than to oxygen O6 of G1. Position of water is controlled by hydrogen bond to N7(G1). In the intermediate state, the aqua ligand is already fully released and does not assist to bond switching from O6 to N7 through TS_2. In TS_2, the chelate ring O6-Ru-N7 is formed and the H-bond between (en) ligand and N7(G2) stabilizes the structure.

Electronic properties

The energy profile of the reaction is shown in Fig. 6 where single point Gibbs free energies from ONIOM model BLYP/6-31G(d)//FF96 are compared with analogous energies of the quantum–core structures in PCM(B3LYP/6-31++G(d,p)). Free energies were calculated based on canonical ensemble of ideal gas with harmonic oscillator approach. Frequency analysis was performed on fully optimized structures. Because DNA structure obtained by optimization procedure dscribed above is very sim-

QM PCM	Reac	Inter	Prod	TS_1	TS_2	TS_{dir}
Ru-C(ben)	2.201	2.110	2.223	2.157	2.150	2.169
Ru-N1(en)	2.159	2.136	2.140	2.168	2.197	2.177
Ru-N4(en)	2.139	2.124	2.156	2.133	2.148	2.177
Ru-O(wat)	2.132	4.172	4.846	2.722	4.284	3.032
Ru-N7(G1)	4.679	3.816	2.172	4.102	2.637	2.862
Ru-O6(G1)	4.257	2.136	3.731	3.106	2.637	4.474
Ru-N7(G2)	4.046	5.326	5.463	6.750	4.507	4.365
Ru-O6(G2)	4.172	4.408	4.615	4.963	4.477	4.294
ONIOM	Reac	Inter	Prod	TS_1	TS_2	TS_{dir}
Ru-C(ben)	2.205	2.186	2.225	2.157	2.150	2.169
Ru-N1(en)	2.144	2.153	2.180	2.133	2.148	2.177
Ru-N4(en)	2.182	2.130	2.146	2.168	2.197	2.177
Ru-O(wat)	2.159	4.481	6.008	2.722	4.070	3.032
Ru-N7(G1)	3.978	3.834	2.201	4.102	2.637	2.862
Ru-O6(G1)	4.707	2.279	3.961	3.009	2.636	4.474
Ru-N7(G2)	4.506	4.697	4.610	6.750	4.507	4.365
Ru-O6(G2)	4.068	3.914	3.846	4.933	4.437	4.262

Table 2: Interatomic distances [Å] in stationary points of reaction where Ru(II) complex is binding to DNA on guanine N7. Direct reaction with single transtion state (TS_{dir}) as well as two step mechanism with intermediate structure (Inter) and two transition states (TS_1, TS_2) is included.

ilar in all stationary points of reaction coordinates, we assume that an error caused by small frequencies in ONIOM model is more or less systematical and cancels in free energy differences. We are aware of weakness of this statement and we hope that our next computational QM/MM model with explicit solvent molecules and umbrella sampling techniques will confirm validity of this approximation. Both the direct reaction with single transition state and two step reaction mechanism are schematically plotted in Fig. 2.

Although the reaction energy is slightly exothermic in QM calculation (-1 kcal/mol), much more pronounced preference for product was obtained in ONIOM model (-12 kcal/mol). Such a large difference can be explained by better stabilization of product structure in ONIOM model where the surrounding DNA structure is included. Also, a hydrogen bond between (en)-H and oxygen on neighbouring cytosine is formed, releasing the water molecule which interacts with negatively charged phosphate group instead of N7(G2) as occurs in QM model. Free energies are very similar for both reaction pathways, that is 26.5 kcal/mol for direct binding and 28 kcal/mol in two–step mechanism. To be sure that they are not influenced by lack of dispersion in BLYP and B3LYP functionals, we recalculated the direct binding path also with more demanding and accurate wB97XD functional. However, difference in

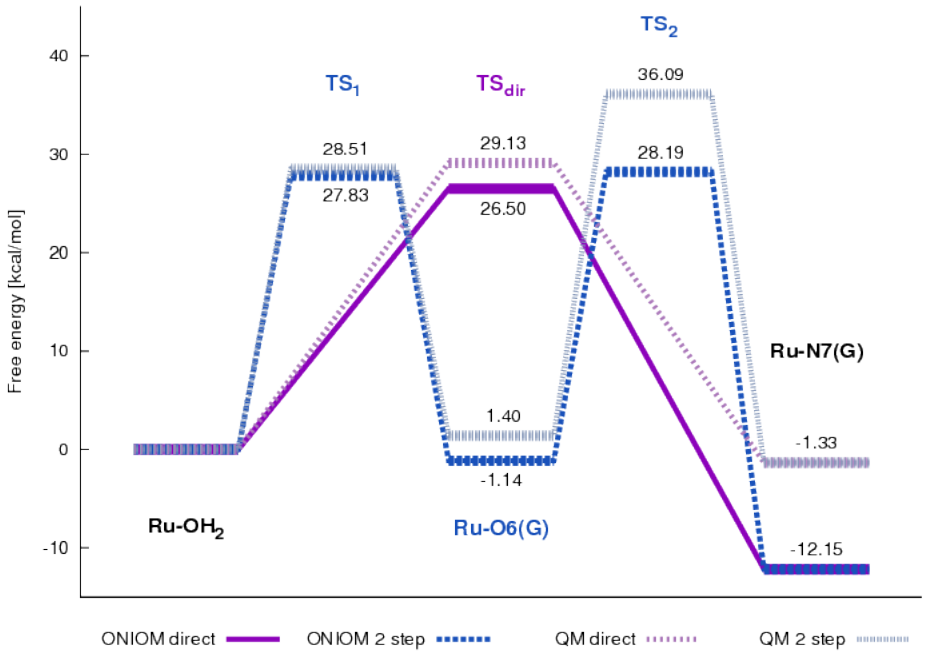

Figure 6: Free energy profile of reaction where the Ru complex binds to DNA on guanine N7 position. Direct as well as two step mechanism is shown (see reaction scheme in Fig. 2 and structures in Fig. 5).

energy barrier is less than 1 kcal/mol. Because this discrepancy is lower than absolute accuracy of our calculations discussed below, we present only B3LYP profiles here that can be easily compared with our previous results.

Conversely, neither implicit nor explicit water solution is involved in ONIOM model, and therefore, overestimation of electrostatic interactions can be expected. Magnitude of this overestimation can be acquired from experimentally obtained rate constant of Ru(II)–OH_2 binding to cGMP, k = (1.13±0.02) $10^{-2}M^{-1}s^{-1}$ [63], which corresponds with barrier $\Delta G \approx$ 20 kcal/mol. Thus, our calculations provide higher energy barriers by about 6 kcal/mol resulting from lack of solvent screening. However, charge of all structures is the same and so qualitatively correct energy profiles can be expected. Results from improved model with explicit water solvent will be presented in our next article where this Ru(II) reaction mechanism will be explored using QM/MM techniques with explicit solvent model.

Interaction energies Binding energies of all the ligands are calculated for optimized QM structures using PCM according to Eq. 1 and their values are displayed in Tab. 3. Strong stabilization of aqua ligand in reactant structure is caused by two hydrogen bonds to O6 oxygens of both guanines, as discussed above. Binding energy of Ru-OH_2 (-38 kcal/mol) can be compared with the similar value of -29 kcal/mol in the isolated Ru(II) complexes [35]. Although in the direct reaction, the aqua ligand is fully released already in transition state structure,

Atoms	Reak	Inter	Prod	TS_1	TS_2	TS_{dir}
Ben	-67.8	-66.2	-67.9	-80.5	-68.1	-77.9
En	-102.9	-109.0	-101.1	-100.5	-95.2	-103.6
Wat	-37.8	-3.4	-6.4	-16.7	-4.1	-5.7
G1	-17.1	-31.4	-40.2	-12.5	-7.9	-8.5
G2	-9.3	-3.9	-5.4	-1.1	-10.2	-16.0

Table 3: Ru–ligand interaction energies [kcal/mol] in complexes of Ru-N7(G) adduct formation reaction (QM, PCM)

it still interacts non-negligibly in TS_1 of the two step mechanism before it is released in intermediate structure.

Coordination of ethylenediamine bidentate ligand is the strongest of all the ligands (ca. 100 kcal/mol) and is practically constant during the reaction. Conversely, interaction energy of η^6–coordinated benzene ligand varies from 67 to 80 kcal/mol and depends on coordination of the remaining ligands to the central Ru cation.

From the last line in Tab. 3, the role of the second guanine, which does not interact covalently with Ru(II) complex can be analyzed. It interacts only weakly in all the complexes of the first reaction step. Association energy varies from 4 to 9 kcal/mol, depending on the type of H–bonding between the guanine and the Ru(II) complex. Conversely, G2 is important for transition state geometry of the direct reaction mechanism, where it helps to keep proper geometry by two H–bonds as discussed above. The G2 has the same function also in TS_2 structure of the two step reaction mechanism. Nevertheless it does not interact with Ru(II) complex in TS_1.

Population analysis NPA population analysis was performed on the optimized stationary points in the QM model at the same level as calculation of interaction energies. The resulting atomic charges are summarized in Tab. 4 where C(ben) means the closest carbon of benzene ring to the Ru(II) cation. The formally 2+ charge on ruthenium is only slightly positive because of electron donation of surrounding ligands. Higher charge on Ru can be seen in transition state structures where aqua ligand and G1 exhibit weaker coordination and donation comes mainly from benzene and ethylenediamine.

Intrastrand CL structure

Intrastrand CL structure is crucial in anticancer activity of cisplatin. As the behaviour and interaction of the Ru(II) complexes with DNA is similar to that metallodrug, it is natural to consider the formation of such a bridging geometry also in case of Ru(II) structures. In contrast to cisplatin, the piano-stool Ru(II) complexes contain only one chloride ligand that can be substituted by water molecule and subsequently by guanine. However, there is also η^6–benzene ligand, whose coordination can be partially released and some valence of the Ru(II) cation reorganized for further interaction.

We consider such a structure reorganization and explore three possible CL ge-

Atom	Reak	Inter	Prod	TS_1	TS_2	TS_{dir}
Ru	0.123	0.040	0.120	0.238	0.154	0.233
C(ben)	-0.172	-0.166	-0.188	-0.179	-0.161	-0.181
N1(en)	-0.744	-0.741	-0.742	-0.777	-0.783	-0.791
N4(en)	-0.748	-0.733	-0.757	-0.762	-0.748	-0.776
O(wat)	-0.880	-1.027	-0.999	-1.007	-1.006	-1.009
N7(G1)	-0.528	-0.415	-0.521	-0.545	-0.525	-0.471
O6(G1)	-0.718	-0.670	-0.592	-0.674	-0.696	-0.698
N7(G2)	-0.510	-0.544	-0.507	-0.514	-0.488	-0.540
O6(G2)	-0.713	-0.680	-0.701	-0.700	-0.630	-0.716

Table 4: NPA atomic charges [e] in complexes of reaction where the Ru complex binds to N7 guanine position in DNA.

ometries, in which Ru(II) cation makes the bridge between two N7 nitrogens on adjacent guanines G1 and G2. Besides these two nucleic bases, the ethylenediamine ligand is always present, and remaining coordination is saturated by benzene and/or aqua ligand. Benzene ligand interacts with Ru by η^2–coordination through one of the ring C–C bonds. Detatching of (en) ligand was not considered because of its strong interaction with central Ru(II) cation known from previous study (ca. 120 kcal/mol [35]).

Structures

Several CL complexes were prepared manually, by modification of optimized Ru-N7(G) adduct on DNA. The preoptimized CL geometries with lowest energies were fully minimized in ONIOM model. Consequently, the quantum–cores structures were reoptimized with constrained positions of both guanines as in case of the previous reaction. The obtained geometries represent stable minima of simulated PES. All relevant interatomic distances characterizing CL geometries are summarized in Tab. 5. The Ru-C(ben) means the distance of the closest carbon of benzene ring to the central Ru(II) cation. Optimized QM cores are shown in Fig. 7 where the pseudo-octahedral coordination of all the geometries is clearly noticeable.

From the Tab. 5, it can be seen that ethylendiamine preserves the same geometry in comparison to the complexes of the previous reaction and it is not influenced by the other ligands within the reaction course. Conversely, the benzene ligand, which is partly released and interacts through one coordination bond only, is further departed from the Ru(II) cation. Binding of both guanines to the Ru(II) complex is not symmetric since G1, which is H–bonded by O6 to H(en-N4) throughout, exhibits shorter Ru-N7 distance.

In the $CL_{W,B}$ both the aqua ligand and benzene are coordinated to the central Ru(II) cation (see Fig. 7c). Aqua ligand further participates in two H–bonds to O6 of both guanines and also ethylendiamine interacts with O6 of G1. Octahedral coordination and η^2–coordination of benzene are apparent not only from geometry parameters but also from AIM analysis.

QM PCM	Ru–G	$CL_{W,B}$	CL_W	CL_B
Ru-C(ben)	2.223	2.576	4.880	2.416
Ru-N1(en)	2.140	2.152	2.136	2.092
Ru-N4(en)	2.156	2.110	2.102	2.127
Ru-O(wat)	4.846	2.173	2.173	4.724
Ru-N7(G1)	2.172	2.096	2.187	2.140
Ru-O6(G1)	3.731	3.750	3.695	2.728
Ru-N7(G2)	5.463	2.275	2.106	2.148
Ru-O6(G2)	4.615	3.781	2.477	3.687
ONIOM	Ru–G	$CL_{W,B}$	CL_W	CL_B
Ru-C(ben)	2.225	2.536	8.575	2.363
Ru-N1(en)	2.180	2.149	2.132	2.111
Ru-N4(en)	2.146	2.121	2.145	2.148
Ru-O(wat)	6.008	2.172	2.215	4.789
Ru-N7(G1)	2.201	2.260	2.085	2.107
Ru-O6(G1)	3.961	3.595	2.396	2.574
Ru-N7(G2)	4.610	2.180	2.194	2.226
Ru-O6(G2)	3.846	3.728	3.749	3.723

Table 5: Interatomic distances [Å] in complexes where the Ru cation interacts with one guanine only (Ru–G) or forms the cross–link geometry (CL). In latter case aqua ligand (W), benzene (B) or both of them (W,B) interacts with Ru.

In other two types of CL geometries, only aqua ligand (CL_W, Fig. 7b) or benzene (CL_B, Fig. 7d) interacts with the Ru(II) cation while the other is fully released from the complex as follows from distances in Tab. 5. It is shown below that the CL_W structure is energetically the most stable and is regarded as a final product of the reaction processes.

Electronic properties

In Fig. 8, two reaction pathways from initial Ru-N7 adduct (i.e. product of previously discussed reaction) to final CL_W cross–link are shown in schematic energy profile. Both pathways represent a two step reaction mechanism and differ in intermediate state that can be $CL_{W,B}$ or CL_B. Again, the ONIOM results are compared with re-optimized QM cores. Heights of energy barriers are obtained from energies of transition states where presence of one imaginary frequency corresponding with antisymmetric stretching vibrational mode was checked (shown in Fig. 7). Contributions to free energy are calculated from vibrational analysis and canonical ensemble of ideal gas.

All the CL structures are in ONIOM model energetically lower than single guanine adduct, demonstrating that they are thermodynamically preferred (cf. Fig. 8). Total reaction Gibbs free energy of CL_W formation is -21 kcal/mol. However, the reaction is kinetically inhibited by a high energy barrier between reactant and interme-

diate structure, which corresponds to large conformational changes in the complex. As can be seen in Fig. 8, formation of $CL_{W,B}$ is blocked by barrier 30 kcal/mol while the activation energy for the CL_B complex is only 24 kcal/mol. Moreover, barrier between CL_B and CL_W is much lower then the barrier from $CL_{W,B}$ (2 kcal/mol vs. 10 kcal/mol). From this comparison, it is apparent that the pathway through the CL_B intermediate is kinetically preferred.

Interaction energies In analogy to the previous reaction, binding energies of optimized CL structures are calculated by the same computational procedure. These values are summarized in Tab. 6 where, for the sake of easier comparison, energy decomposition of the Ru-N7(G1) adduct is shown as well. The binding energy of ethylenediamine chelate ring is practically constant due to strong coordination to Ru(II) through nitrogens N1 and N4, and H–bonding to O6 of G1. On the contrary, benzene interaction is reduced rapidly from initial 68 kcal/mol corresponding to η^6–coordination to 17 kcal/mol in CL_B and 12 kcal/mol in $CL_{W,B}$. These smaller values can be easily understood by interaction of Ru(II) with only one C–C bond of benzene ring. The AIM analysis shows that two neighbouring carbons participate in the Ru–benzene interaction, which suggests η^2–coordination. The benzene ligand is finally fully released in the CL_W structure.

The water molecule that interacts with Ru directly in complexes $CL_{W,B}$ and CL_W is bound not so strongly as in reactant of the Ru-N7(G) adduct formation reaction (Fig. 2). The difference of the corresponding binding energies is about 10 kcal/mol, which represents about 30% reduction of the original Ru–O(Aq) coordination. In CL_W this is because the aqua ligand interacts only with the Ru(II) cation and does not participate in any hydrogen bond (cf. Tab. 7 below). In contrast, binding situation of aqua ligand in $CL_{W,B}$ is similar to the initial reactant, but AIM analysis reveals that all interactions of this complex (to Ru and both O6 oxygens) are weaker and the difference of sums of electron densities on related bond critical points (BCPs) is 0.02 $e/Å^3$, which corresponds to the fact that stronger coordination of both N7(G) sites competes the Ru–O(Aq) bonding. The similar picture follows also from ETS–NOCV analysis performed on QM core structures. Comparing the Ru–O values in Tab. 7b analogous difference is visible. In Tab. 7 interaction energies of water lignad in all reactants and products from both binding and cross–linking reactions are collected. From the first part of Tab. 7, it clearly follows very strong symmetrical H–bonding interaction of aqua–ligand with both guanine bases (ca. 10 kcal/mol). The Ru–O coordination is predicted to be 36 kcal/mol, which is in fair agreement with binding energy determined in QM model in Tab. 6. In the product state of adduct formation, water molecule is released from Ru(II) complex. The H–bond $H_2O\ldots O6(G1)$ interaction is about 6 kcal/mol (plus 3 kcal/mol for water…benzene interaction).

In all the considered CL structures, the Ru(II) complex interacts with both guanines. Asymmetry in guanine interaction energies in $Cl_{W,B}$ and CL_W is caused by different bonding arrangements. Although in $Cl_{W,B}$ G1 coordinates to Ru more strongly than G2, because of hydrogen bond to ethylendiamine, in Cl_W the coordination of Ru(II) to O6 of G2 can be traced – clearly approaching to the O6, N7–chelate bonding pattern (cf. also the interatomic distances

Atoms	Ru-G	$CL_{W,B}$	CL_W	CL_B
Ben	-67.9	-11.6	0.3	-17.5
En	-101.1	-95.5	-101.3	-106.8
Wat	-6.4	-28.2	-23.3	-3.1
G1	-40.2	-47.0	-35.4	-41.5
G2	-5.4	-35.9	-46.5	-42.4

Table 6: Ru–ligand interaction energies [kcal/mol] in complexes of cross–link structures (CL) and single guanine interaction complex (Ru-G) calculated in QM model with PCM.

free Ru-OH_2 + G		Ru-N7(G) adduct	
Ru–O	-35.74	N7(G2)...O	-5.96
asym (O)–H...O6	-9.89	H(ben)...O	-3.45
sym (O)–H...O6	-9.80		

(a) Ru-N7(G) adduct formation

$CL_{W,B}$		CL_W		CL_B	
Ru–O	-27.70	Ru–O	-21.10	(G2)O6...H(aq)	-2.59
(O)–H...O6(G1)	-10.83	Ru–O	-2.03	(aq)O...H(ben)	-0.63
(O)–H...O6(G2)	-4.36	Ru–O–N7O6(G2)	-1.61		
(O)–H...O6(G1)	-1.56				

(b) cross–link formation

Table 7: ETS–NOCV energy decomposition for interaction of aqua ligand in all reactant and product complexes.

in Tab. 5). Finally, in the Cl_B intermediate structure, both these effects are balanced and the guanine binding energies are almost equal.

Interesting features are visible for cross–link complexes from the ADF energy decomposition. In the $CL_{W,B}$ and CL_W structures where water is directly coordinated to Ru complex, clear verification of the results in Tab. 6 discussed in previous paragraph can be noticed. More over it can be also seen the asymmetric H–bonding of both guanines. While in CL_W water interacts only with G2, in the $CL_{W,B}$ structure the aqua lignad interacts with O6 of the both guanines but in highly non-symmetrical manner as is demonstrated in Tab. 7.

Based on the thermodynamic considerations, the CL_W structure is the final product of the regarded reaction. Despite the fact that in consequent steps, the aqua–ligand will be with very high probability replaced by some more stable lignad, we can compare the coordination strenght to both guanines. Similarly to cisplatin coordination also in Ru(II) case 3'-end guanine is the base which is more firmly attached to metal cation. In the CL_W complex the preference for G2 is

about 10 kcal/mol while in cisplatin complex the energy difference is ca 5 kcal/mol [64]. However, the comparison is not straightforward since different model environment (gas phase calculations) was used in study.

Wave function analysis Atomic partial charges calculated on optimized QM cores in PCM using NPA method are presented in Tab. 8. In accord to interaction energies and population analysis on complexes in the first reaction, the charges on nitrogens in ethylendiamine practically do not vary and a small asymmetry is caused by different participating in hydrogen bonding. Although the charge on oxygen in aqua ligand is close to -1 e in non-interacting water molecule, significantly higher values appear in $CL_{W,B}$ and CL_W where the lone electron–pairs of oxygen donate to the central Ru(II) cation.

Interesting changes can be seen on carbons in benzene ring. In all the CL structures the charge is more negative than in complexes of the first reaction where the benzene ligand is symmetrically η^6–coordinated. The difference is ca 0.06 e, and directly corresponds to weaker interaction with the Ru(II) cation since electron density is not donated to the metal and remains on carbon atoms.

AIM analysis was done on thereoptimized QM cores. Electron densities in BCP between the Ru(II) cation and its ligands were calculated by AIMAll software and are shown in Tab. 9 and Tab. 10. Reaction mechanism of binding hydrated Ru(II)–OH_2 complex to N7(G1) can be observed from BCPs in Tab. 9. There is transition state for direct path (TS_{dir}) where the Ru(II) cation interacts weakly with both aqua ligand and N7(G1). Conversely, in the two–step mechanism, Ru(II) complex first passes through TS_1 to O6(G1), which is in the next step rebondd to N7(G1) through TS_2 structure. Both BCPs between Ru–O6 and Ru–N7 can be seen in AIM analysis of TS_2.

More complicated reaction changes occur in cross–linke reaction mechanism as can be noticed from AIM analysis of related stationary points (Tab. 10). To create new bond to N7(G2) (and thus, to form the (G1)N7–Ru–N7(G2) cross–linked structure), the η^6–coordination of benzene ligand is transformed to η^2–one. In this way, the total coordination number of Ru(II) is kept to be 6. The bond reorganization is illustrated by BCPs in TS_{1a} and TS_{2a} where the arene ligand already interacts with Ru(II) by two carbons only. In these transition state structures, new BCP between Ru–N7(G2) can be already established. To saturate free valence on Ru(II) in CL_B, where water ligand does not participated in the complex, O6(G2) is also involved in the interaction. The same O6(G2) can be found in final CL_W structure where benzene is completely released and substituted by water.

Conclusions

First, the reaction by which a Ru(II) "piano–stool" aqua complex binds to DNA was studied by hybrid QM/MM computational technique coupling DFT and Amber FF96. The Ru(II) complex and two adjacent guanines of one DNA strand are included in the QM part of the system, allowing comparison of direct and two step reaction mechanisms. Two step mechanism is discriminated by high energy barrier of second step, involving Ru(II) binding switching from O6 to N7 of the guanine. This is in contrast with our previous results [35] where the same reaction was studied by QM methods and the model in-

Atom	Ru-G	$CL_{W,B}$	CL_W	CL_B
Ru	0.120	0.240	0.322	0.298
C(ben)	-0.188	-0.256	-0.249	-0.266
N1(en)	-0.742	-0.764	-0.788	-0.713
N4(en)	-0.757	-0.758	-0.730	-0.784
O(wat)	-0.999	-0.899	-0.867	-1.021
N7(G1)	-0.521	-0.406	-0.437	-0.446
O6(G1)	-0.592	-0.697	-0.680	-0.614
N7(G2)	-0.507	-0.449	-0.437	-0.433
O6(G2)	-0.701	-0.681	-0.609	-0.701

Table 8: NPA atomic charges [e] in sigle guanine interaction complex and cross–link structures (QM, PCM).

cluded only one guanine. From that, we can deduce that the molecular environment is important for correct description of the reaction mechanism and QM/MM approach including part of DNA structure seems to be more appropriate. Formation of the adduct to N7 guanine is energetically preferred by 12 kcal/mol but the relatively high barriers, (ca. 28 kcal/mol both), inhibit the process kinetically.

In the second part, in analogy to cisplatin, the possible intrastrand CL structures are suggested and their stability investigated. Although a vast reorganization of the structure is needed to create bridging geometry, these structures are energetically preferred in QM/MM model. All main active position of both guanines (O6 and N7 atoms) participate in Ru(II) complex interactions with DNA, leading to very stable structure with psedo–octahedral symmetry. There are two reaction pathways leading to the energetically lowest structure, CL_W. First one, passing through $CL_{W,B}$ structure, is inhibited by high energy barrier 30 kcal/mol while the second one, with CL_B intermediate, has a barrier of 24 kcal/mol. Although the CL_B structure is energetically higher than $CL_{W,B}$ (by 3 kcal/mol), this pathway is preferred kinetically.

Acknowledgements

The authors (JVB and ZF) are grateful for support provided by the MŠMT GAČR Grant Project MS0021620835, ME10149, and by GAČR Grant Project P205/10/0228. JAP is grateful to the Leverhulme Trust for a Research Fellowship. Authors are also thankful for computational time obtained in Supercomputer Metacenters in Prague and Brno.

References

[1] Reedijk, J. *Curr. Opin. Chem. Biol.*, **3**(2):236 – 240, 1999.

[2] Ronconi, L. and Sadler, P.J. *Coord. Chem. Rev.*, **251**(13-14):1633 – 1648, 2007. 37th International Conference on Coordination Chemistry, Cape Town, South Africa.

[3] Lippert, B., editor. *Cisplatin: Chemistry and Biochemistry of a Leading Anticancer*

Bond		Reak	Inter	Prod	TS_1	TS_2	TS_{dir}
Ben	Ru-C1	8.23	7.46	7.72	6.97	—	—
	Ru-C2	8.02	—	7.86	—	—	8.96
	Ru-C3	—	8.38	—	8.99	8.89	8.77
	Ru-C4	—	8.19	7.31	9.20	9.29	—
	Ru-C5	7.74	—	7.41	—	—	—
	Ru-C6	—	7.36	7.74	7.36	7.77	7.47
En	Ru-N1	8.41	9.01	8.88	9.19	8.83	8.27
	Ru-N4	8.90	9.38	8.44	8.49	7.96	8.27
Wat	Ru-O	7.30	—	—	2.19	—	1.57
G1	Ru-N7	—	—	7.61	—	3.17	—
	Ru-O6	—	6.74	—	6.74	2.84	—
G2	Ru-N7	—	—	—	—	—	2.05
	Ru-O6	—	—	—	—	—	—

Table 9: Electron density [10^{-2} $e/Å^3$] in important BCPs of complexes of reaction where the Ru complex binds to N7 guanine position in DNA.

Drug. Wiley-VCH Verlag GmbH, Wienheim, Germany, 1999.

[4] Rosenberg, B.; van Camp, L.; and Krigas, T. *Nature*, **205**:698–6999, 1965.

[5] Wheate, N.J.; Walker, S.; Craig, G.E.; and Oun, R. *Dalton Trans.*, **39**:8113–8127, 2010.

[6] Perez, R.P. *Eur. J. Cancer*, **34**:1535–1542, 1998.

[7] Canetta, R.; Rozencweig, M.; and Carter, S.K. *Cancer Treat Rev.*, **12**:125–136, 1985.

[8] Graham, J.; Mushin, M.; and Kirkpatrick, P. *Nat. Rev. Drug. Discov.*, **3**:11–12, 2004.

[9] Hindmarsch, K.; House, D.A.; and Turnbull, M.M. *Inorg. Chim. Acta*, **257**(1):11 – 18, 1997.

[10] Marzilli, L.G.; Ano, S.O.; Intini, F.P.; and Natile, G. *J. Am. Chem. Soc.*, **121**:9133–9142, 1999.

[11] Mikola, M. and Arpalahti, J. *Inorg. Chem.*, **33**:4439–4445, 1994.

[12] Miller, S.E.; Gerard, K.J.; and House, D.A. *Inorg. Chim. Acta*, **190**(1):135 – 144, 1991.

[13] Burda, J.V.; Zeizinger, M.; and Leszczynski, J. *J. Chem. Phys.*, **120**(3):1253–1262, 2004.

[14] Burda, J.V.; Zeizinger, M.; and Leszczynski, J. *J. Comput. Chem.*, **26**:907–914, 2005.

[15] Baik, M.H.; Friesner, R.A.; and Lippard, S.J. *J. Am. Chem. Soc.*, **125**(46):14082–14092, 2003.

[16] Chval, Z. and Šíp, M. *Collection Czechoslovak Chem. Communications*, **68**(6):1105–1118, 2003.

[17] Deubel, D.V. *J. Am. Chem. Soc.*, **128**(5):1654–1663, 2006.

[18] Dos Santos, H.F.; Marcial, B.L.; De Miranda, C.F.; Costa, L.A.S.; and De Almeida, W.B. *J. Inorg. Biochem.*, **100**(10):1594–1605, 2006.

[19] Lau, J.K.C. and Deubel, D.V. *J. Chem. Theory and Computation*, **2**(1):103–106, 2006.

[20] Pavankumar, P.N.; Seetharamulu, P.; Yao,

S.; Saxe, J.D.; Reedy, D.G.; and Hausheer, F.H. *J. Comput. Chem.*, **20**(3):365–382, 1999.

[21] Raber, J.; Zhu, C.; and Eriksson, L.A. *J. Phys. Chem. B*, **109**:11006–11015, 2005.

[22] Robertazzi, A. and Platts, J.A. *Chem. Eur. J.*, **12**(22):5747–5756, 2006.

[23] Zhang, Y.; Guo, Z.; and You, Z.Z. *J. Am. Chem. Soc.*, **123**:9378–9387, 2001.

[24] Zimmermann, T. and Burda, J.V. *Dalton Trans.*, **39**:1295–1301, 2010.

[25] Pascoe, J.M. and Roberts, J.J. *Biochem. Pharmacol.*, **23**(9):1345 – 1357, 1974.

[26] Cohen, S.M.; Mikata, Y.; He, Q.; and Lippard, S.J. *Biochemistry*, **39**(38):11771–11776, 2000.

[27] Iwamoto, M.; Mukundan, S.; and Marzilli, L.G. *J. Am. Chem. Soc.*, **116**(14):6238–6244, 1994.

[28] Malina, J.; Novakova, O.; Keppler, B.K.; Alessio, E.; and Brabec, V. *J. Biol. Inorg. Chem.*, **6**:435–445, 2001.

[29] Takahara, P.M.; Frederick, C.A.; and Lippard, S.J. *J. Am. Chem. Soc.*, **118**(49):12309–12321, 1996.

[30] Allardyce, S.C. and Dyson, J.P. *Platinum Metals Review*, **45**(2):62–69, 2001.

[31] Morris, R.E.; Aird, R.E.; del Socorro Murdoch, P.; Chen, H.; Cummings, J.; Hughes, N.D.; Parsons, S.; Parkin, A.; Boyd, G.; Jodrell, D.I.; and Sadler, P.J. *J. Med. Chem.*, **44**(22):3616–3621, 2001.

[32] Aird, R.; Cummings, J.; Ritchie, A.A.; Muir, M.; Morris, R.E.; Chen, H.; Sadler, P.J.; and Jodrell, D.I. *Br. J. Cancer*, **86**:1652–1657, 2002.

[33] Guichard, S.; Else, R.; Reid, E.; Zeitlin, B.; Aird, R.; Muir, M.; Dodds, M.; Fiebig, H.; Sadler, P.; and Jodrell, D. *Biochem. Pharm.*, **71**(4):408 – 415, 2006.

[34] Deubel, D.V. and Kai-Chi Lau, J. *Chem. Comm.*, **23**:2451–2453, 2006.

[35] Futera, Z.; Klenko, J.; Sponer, J.E.; Sponer, J.; and Burda, J.V. *J. Comput. Chem.*, 2009.

[36] Fernández, R.; Melchart, M.; Habtemariam, A.; Parsons, S.; and Sadler, P.J. *Chem. Eur. J.*, **10**:5173–5179, 2004.

[37] Brabec, V. and Novakova, O. *Drug. Res. Upd.*, **9**(3):111 – 122, 2006.

[38] Pizarro, A.M. and Sadler, P.J. *Biochimie*, **91**:1198–1211, 2009.

[39] Wang, F.; Chen, H.; Parsons, S.; Oswald, I.D.H.; Davidson, J.E.; and Sadler, P.J. *Chem. Eur. J.*, **9**:5810–5820, 2003.

[40] Gossens, C.; Tavernelli, I.; and Rothlisberger, U. *J. Phys. Chem. A*, **113**:11888–11897, 2009.

[41] Case, D.A.; Darden, T.A.; Cheatham, T.E.; Simmerling, C.L.; Wang, J.; E., D.R.; Luo, R.; Merz, K.M.; Wang, B.; Pearlman, D.A.; Crowley, M.; Brozell, S.; Tsui, V.; Gohlke, H.; Mongan, J.; Hornak, V.; Cui, G.; Beroza, P.; Schafmeister, C.; Caldwell, J.W.; Ross, W.S.; and Kollman, P.A. Amber 8, 2004. University of California, San Francisco.

[42] Cornell, W.D.; Cieplak, P.; Bayly, C.I.; Gould, I.R.; Merz, Jr., K.M.; Ferguson, D.M.; Spellmeyer, D.C.; Fox, T.; James Caldwell, J.W.; and Kollman, P.A. *J. Am. Chem. Soc.*, **117**:5179–5197, 1995.

[43] Kollman, P.A. *Acc. Chem. Res.*, **29**:461–469, 1996.

[44] Jorgensen, W.L.; Chandrasekhar, J.; Madura, J.D.; Impey, R.W.; and Klein, M.L. *J. Chem. Phys.*, **79**(2):926–935, 1983.

[45] Grest, G.S. and Kremer, K. *Phys. Rev. A*, **33**(5):3628–3631, 1986.

[46] Dapprich, S.; Komaromi, I.; Byun, K.S.; Morokuma, K.; and Frish, M.J. *J. Mol. Struct. (Theochem)*, **462**:1, 1999.

[47] Svensson, M.; Humbel, S.; Froese, R.D.J.;

Matsubara, T.; Sieber, S.; and Morokuma, K. *J. Phys. Chem.*, **100**:19357–19363, 1996.

[48] Frisch, M.J.; Trucks, G.W.; Schlegel, H.B.; Scuseria, G.E.; Robb, M.A.; Cheeseman, J.R.; Scalmani, G.; Barone, V.; Mennucci, B.; Petersson, G.A.; Nakatsuji, H.; Caricato, M.; Li, X.; Hratchian, H.P.; Izmaylov, A.F.; Bloino, J.; Zheng, G.; Sonnenberg, J.L.; Hada, M.; Ehara, M.; Toyota, K.; Fukuda, R.; Hasegawa, J.; Ishida, M.; Nakajima, T.; Honda, Y.; Kitao, O.; Nakai, H.; Vreven, T.; Montgomery, Jr., J.A.; Peralta, J.E.; Ogliaro, F.; Bearpark, M.; Heyd, J.J.; Brothers, E.; Kudin, K.N.; Staroverov, V.N.; Kobayashi, R.; Normand, J.; Raghavachari, K.; Rendell, A.; Burant, J.C.; Iyengar, S.S.; Tomasi, J.; Cossi, M.; Rega, N.; Millam, N.J.; Klene, M.; Knox, J.E.; Cross, J.B.; Bakken, V.; Adamo, C.; Jaramillo, J.; Gomperts, R.; Stratmann, R.E.; Yazyev, O.; Austin, A.J.; Cammi, R.; Pomelli, C.; Ochterski, J.W.; Martin, R.L.; Morokuma, K.; Zakrzewski, V.G.; Voth, G.A.; Salvador, P.; Dannenberg, J.J.; Dapprich, S.; Daniels, A.D.; Farkas, O.; Foresman, J.B.; Ortiz, J.V.; Cioslowski, J.; and Fox, D.J. Gaussian 09, Revision A.01, 2009. Gaussian, Inc., Wallingford, CT.

[49] Andrae, D.; Häußermann, U.; Dolg, M.; Stoll, H.; and Preuß, H. *Theor Chim Acta*, **77**:123–141, 1990.

[50] Bergner, A.; Dolg, M.; Kuumlchle, W.; Stoll, H.; and Preuß, H. *Mol Phys*, **80**:1431–1441, 1993.

[51] Bader, R.F.W. *Pure Appl. Chem.*, **60**(2):145–155, 1988.

[52] Bader, R.F.W. and Essen, H. *J. Chem. Phys.*, **80**(5):1943–1960, 1984.

[53] Bader, R.F.W. *Atoms in Molecules: A Quantum Theory*. Clarendon Press, Oxford, U.K., 1990.

[54] Keith, T.A. AIM All, 2009.

[55] Glendening, E.D.; Badenhoop, K.; Ree, A.E.; Carpenter, J.E.; Bohmann, J.A.; Morales, M.; and Weinhold, F. NBO 5.0, 2001. Theoretical Chemistry Institute, University of Wisconsin, Madison.

[56] Reed, A.E.; Weinstock, R.B.; and Weinhold, F. *J. Chem. Phys.*, **83**:735–746, 1985.

[57] Mitoraj, M.; Michalak, A.; and Ziegler, T. *J. Chem. Theor. Comput.*, **5**:962, 2009.

[58] Ziegler, T. and Rauk, A. *Theor. Chim. Acta*, **46**:1–8, 1977.

[59] Michalak, A.; Mitoraj, M.; and Ziegler, T. *J. Phys. Chem. A*, **112**(9):1933–1944, 2008.

[60] Mitoraj, M. and Michalak, A. *J. Mol. Model.*, **13**:347–354, 2007.

[61] Baerends, E.J.; Autschbach, J.; Bashford, D.; Berces, A.; Bickelhaupt, F.M.; Bo, C.; Boerrigter, P.M.; Cavallo, L.; Chong, D.P.; Deng, L.; Dickson, R.M.; Ellis, D.E.; Faassen, M.v.; Fan, L.; Fischer, T.H.; Fonseca Guerra, C.; Ghysels, A.; Giammona, A.; Gisberger, S.J.A.v.; Gotz, A.W.; Groeneveld, J.A.; Gritsenko, O.V.; Gruning, M.; Harris, F.E.; Hoek, P.v.d.; Jacob, C.R.; Jacobsen, H.; Jensen, L.; Kessel, G.v.; Kootstra, F.; Krykunov, M.V.; Lenthe, E.v.; McCormack, D.A.; Michalak, A.; Mitoraj, M.; Neugebauer, J.; Nicu, V.P.; Noodleman, L.; Osinga, V.P.; Patchkovskii, S.; Philipsen, P.H.T.; Post, D.; Pye, C.C.; Ravenek, W.; Rodriguez, J.I.; Ros, P.; Schipper, P.R.T.; Schreckenbach, G.; Seth, M. Snijders, J.G.; Mola, M.; Swart, M.; Swerhone, D.; Velde, G.t.; Vernooijs, P.; Versluis, L.; Visscher, L.; Visser, O.; Wang, F.; Wesolowski, T.A.; Wezenbeek, E.M.v.; Wiesenekker, G.; Wolff, S.K.; Woo, T.K.; Yakovlev, A.L.; and Ziegler, T. ADF2009, 2009. Theoretical Chemistry, Vrije Universiteit, Amsterdam, The Netherlands, http://www.scm.com.

[62] Becke, A.D. *J. Chem. Phys.*, **88**:1053–1062, 1988.

[63] Chen, H.; Parkinson, J.A.; Morris, R.E.; and Sadler, P.J. *J. Am. Chem. Soc.*, **125**:173–186, 2003.

[64] Zeizinger, M.; Burda, J.V.; and Leszczynski, J. *Phys. Chem. Chem. Phys.*, **6**(10):3585–3590, 2004.

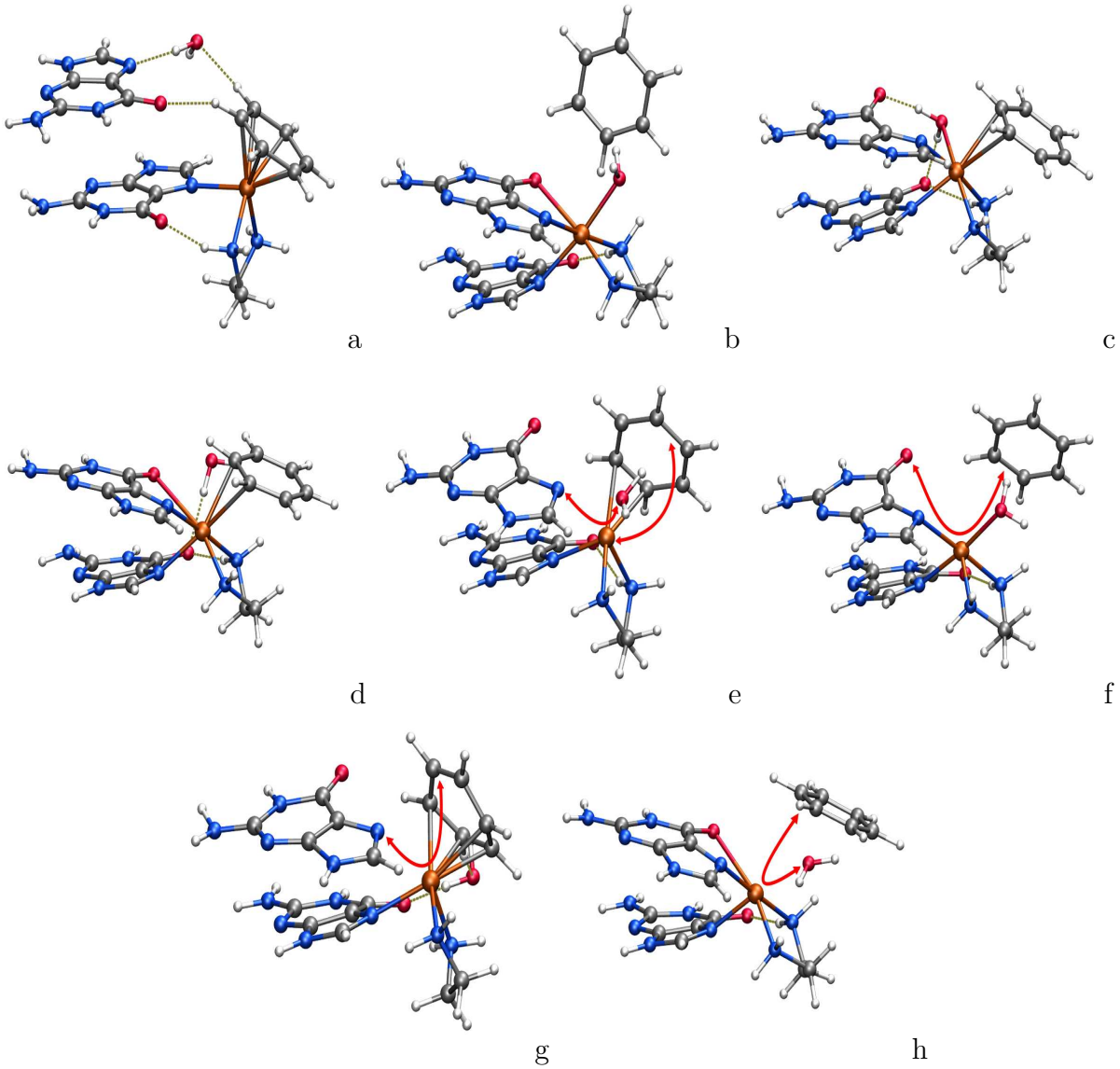

Figure 7: Optimized cross–link structures (see reaction scheme in Fig. 3): (a) Ru-N7(G) adduct, (b) CL_W, (c) $CL_{W,B}$, (d) CL_B, (e) TS_{1a}^{CL}, (f) TS_{1b}^{CL}, (g) TS_{2a}^{CL}, (h) TS_{2b}^{CL}.

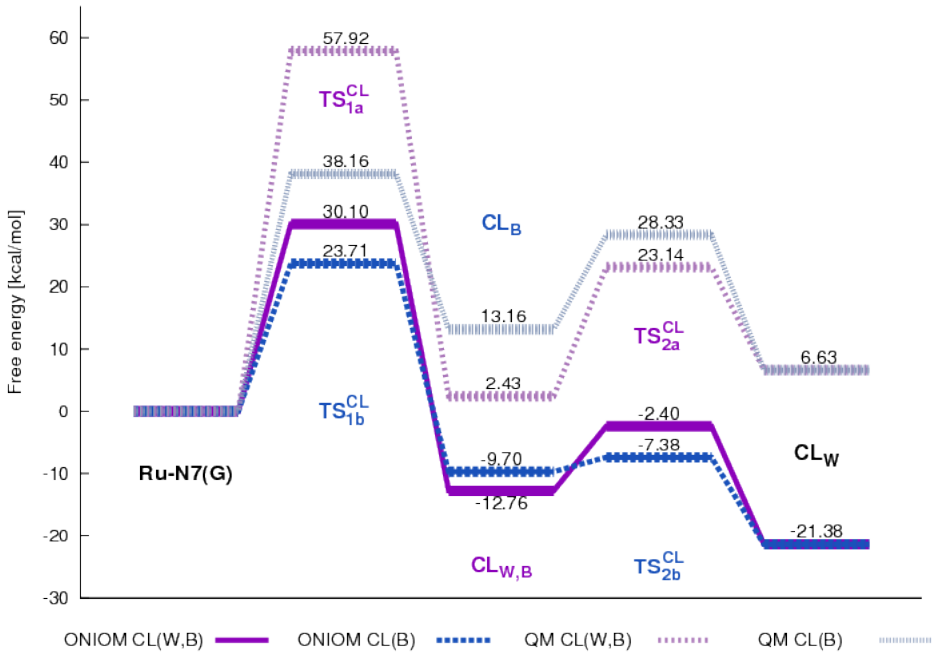

Figure 8: Free energy profile of reaction where the cross–link structure is formed. Three type of cross–links are considered with interacting benzene (B), water (W) or both of them (W,B).

Bond		Ru-G	$CL_{W,B}$	CL_W	CL_B
Ben	Ru-C1	7.72	—	—	5.22
	Ru-C2	7.86	3.44	—	4.02
	Ru-C3	—	2.94	—	—
	Ru-C4	7.31	—	—	—
	Ru-C5	7.41	—	—	—
	Ru-C6	7.74	—	—	—
En	Ru-N1	8.88	8.95	8.54	8.77
	Ru-N4	8.44	8.10	9.02	9.45
Wat	Ru-O	—	6.29	5.86	—
G1	Ru-N7	7.61	8.66	6.95	7.77
	Ru-O6	—	—	—	—
G2	Ru-N7	—	5.51	8.11	7.64
	Ru-O6	—	—	3.30	2.19

Table 10: Electron density [10^{-2} $e/Å^3$] in important BCPs of single guanine interaction complex and cross–link structures (QM, PCM).